Geogenic greenhouse gas emissions and shale weathering: lessons learned from an alpine “eternal flame”

Michaela Blessing, Catherine Lerouge, Frédérick Gal, Abdeltif Lahfid, Christine Flehoc, W. Kloppmann

Science of the Total Environment 987 (2025) 179799

Contents lists available at ScienceDirect

Science of the Total Environment

journal homepage: www.elsevier.com/locate/scitotenv

Geogenic greenhouse gas emissions and shale weathering: lessons learned from an alpine "eternal flame"

M. Blessing *, C. Lerouge, F. Gal, A. Lahfid, C. Fléhoc, W. Kloppmann

BRGM, French Geological Survey, Orléans, France

HIGHLIGHTS

- Geogenic gas emissions can increase concentrations of greenhouse gases in atmosphere.
- Natural gas releases in orogenetic belts and weathering black shales occur worldwide.
- Complex interaction of physical, geochemical, microbial and hydrological conditions
- Rock degassing studies give evidence of processes controlling diffuse gas emissions.
- Isotopic data inform on maturation and ongoing post-genetic secondary processes.

GRAPHICAL ABSTRACT

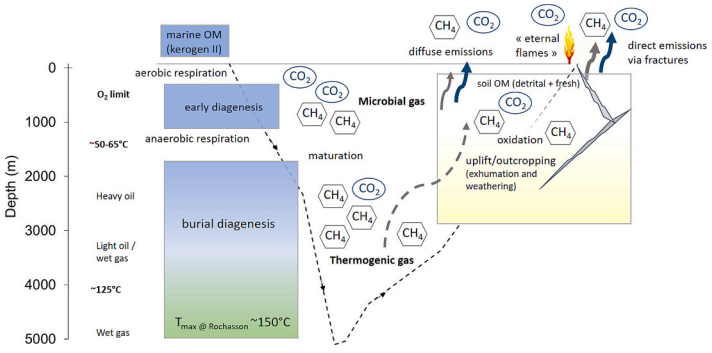

ARTICLE INFO

Editor: Christian Herrera

Keywords:
Isotope geochemistry
Methane
Carbon dioxide
Shale gas
CH4 consumption
Environmental geology
French Alps

ABSTRACT

Natural hydrocarbon gas seeps have been reported over a wide range of geological settings, and their contribution to atmospheric concentrations of potent greenhouse gases (CO_2, CH_4) may be considerable. Potential gas sources in sedimentary environments include organic-rich source rocks such as peats, coalbeds, and shale clays. The origins of natural methane seepages occurring in the French Subalpine Chains are poorly constrained and only little information is available on the mechanisms behind the gas release by weathering of organic-rich shales, notably when overprinted by recent tectonism. The investigated site, where outcropping Callovian-Oxfordian black shales emit methane, higher alkanes and CO_2 through macro- and micro-seeps, shows the complexity of these mechanisms. We report geochemical, isotopic and petrographic data from the Meylan-Rochasson eternal flame site, from in-situ measurements, gas, pore water and sediment sampling and degassing experiments, and propose a conceptual model covering all stages of reservoir evolution from early diagenesis to exhumation and weathering. Rock degassing experiments under helium allowed extracting alkanes and CO_2 dissolved in pore waters. Isotopic signatures from below 20–40 cm are comparable to the macro-seep, indicating a common thermogenic origin of alkanes through maturation of organic matter at ~150 °C. Secondary methane oxidation processes affect both point- and diffuse emissions of thermogenic methane. In the pore waters of outcropping shales and colluvium thermogenic gas mix with a microbial methane component. This superposition of weathering, oxidation of OM and microbially driven processes needs to be considered in future studies investigating the importance of direct natural gas emission from shales worldwide.

* Corresponding author at: BRGM, DE/QES, 3 avenue Claude Guillemin, F-45060 Orléans, France.
E-mail address: m.blessing@brgm.fr (M. Blessing).

https://doi.org/10.1016/j.scitotenv.2025.179799
Received 1 April 2025; Received in revised form 26 May 2025; Accepted 28 May 2025
Available online 4 June 2025

1. Introduction

Methane is one of the trace gases in atmosphere that plays a major role on the global greenhouse effect being 28 times more powerful than CO_2. Global CH_4 emissions have been estimated to ~500–600 million tonnes CH_4 per year (Mt. yr^{-1}) (Conrad, 2009; Saunois et al., 2017). Around 60 % of these emissions are due to human activity (anthropogenic), while about 40 % come from natural methane sources (IAE, 2023). Important quantities of methane emissions originate from microbial activity in wetland environments and freshwater lakes (Borrel et al., 2011; Venturi et al., 2021; Wang et al., 1996). Geological emissions are significant, esp. from oceanic gas hydrates under the effects of climate change, seeps in petroleum-bearing sedimentary basins or in volcanic and geothermal areas (Etiope et al., 2009a, 2007; Etiope and Klusman, 2002; James et al., 2016; Ruppel and Kessler, 2017). Estimates for global geological CH_4 release are controversial and range from ~1.6 Mt. yr^{-1} to ~45 Mt. yr^{-1} (Hmiel et al., 2020; Mazzini et al., 2021). Abiotic sources involve magmatic degassing including volcanic emissions and igneous rock degassing, hydrothermal sources but also alteration processes of ultramafic rocks (Etiope and Sherwood Lollar, 2013). Thermogenic methane is linked to catagenic hydrocarbon-generation processes in organic matter-rich rocks, such as conventional (sandstone and limestone) and unconventional (shales) petroleum reservoirs in sedimentary basins (Etiope et al., 2013, 2009a). Apart from these primary sources, secondary microbial gases by anaerobic biodegradation of hydrocarbons can be present (Etiope et al., 2009b; Gong et al., 2017; James and Burns, 1984). Natural CO_2 and CH_4 gas emissions can thus have different sources and migration pathways. The pathways of methane emissions depend on the geological context and the gas sources. Direct emissions are from volcanoes, surficial emissions through soils and sediments (micro-seeps), and deeper emissions through fracture networks developed at different scales of the crust (macro-seeps) (Etiope, 2015). Fracture networks are associated to weathering processes developed in the critical zone (Ding et al., 2012; Lachassagne et al., 2011), and to faults created in active tectonic environments that act as pathways for gas seepage (Etiope and Klusman, 2002; Klusman, 2018; Sugisaki et al., 1980).

The Jurassic "Terres Noires" shales of SE France are a marine clay formation rich in organic matter, attributed to the Callovian Oceanic Anoxic Event (Jenkyns et al., 2002), with outcrops along the southern Subalpine Chains (French Alps). They are well known for their hydrocarbon content (Guilhaumou et al., 1996; Moss, 1992), and occurrence of methane seeps (Blavoux and Dazy, 1990; Etiope et al., 2010; Gal et al., 2018). By their location in the French Alps, the shales underwent deep burial and important deformation during compressional events (Guilhaumou et al., 1996). Due to Quaternary exposure, the shales have undergone erosion and weathering processes, with development of local wetlands that are investigated elsewhere for methane emissions in the particular Alpine environment (Koch et al., 2007). Unlike wetlands where water is retained at the surface, fractured and faulted zones due to Alpine tectonics are favoured areas for infiltration of meteoric fluids at depth, and CH_4 production by degradation of organic matter (Krüger et al., 2014). For all these reasons, the "Terres Noires" shales represent a good target to gain better understanding of the different processes of natural methane production and migration in and from shale gas reservoirs. The two best-known gas seep sites in the "Terres Noires" shales are close to Grenoble in SE France (La Fontaine Ardente at Le Gua and Rochasson at Meylan). They have been studied by flux measurements at the soil/atmosphere interface at the vents and in the surrounding diffuse seepage area and through quantification of free gas concentrations at 1 m depth in the soil (Gal et al., 2017, 2019). Gas flux is highest at La Fontaine Ardente with an emission of ~40–50 kg of CH_4 per day (Gal et al., 2018); however, the seep was modified by the installation of a gasometer to exploit gas in the late XIX^{th} century and subsequent borehole drilling in the 1990s (Berthier et al., 1991; Gal et al., 2018). Although gas emissions are one order of magnitude lower, the Rochasson gas seep was chosen as being more favourable for field gas and laboratory measurements due to direct accessibility to outcropping shales.

The main objectives of this work are to refine the estimates of the natural gas emissions from the "Terres Noires" shales with regard to the Rochasson gas seep, to determine the origins of the gases (thermogenic and/or microbial) and to discuss the main processes, which govern the methane emissions in such a context. The results can serve as reference for investigating methane emissions from similar environments worldwide where important volumes of black shales, matured and fractured by young tectonism, outcrop and potentially release methane to the atmosphere over large surfaces. We performed a thorough petrological and geochemical characterization of the Rochasson "Terres Noires" shales, to define their diagenetic sequence, the burial conditions and the weathering processes of the shales. A new flux measurements campaign was carried out to assess the evolution of the gas seep since our first investigations (Gal et al., 2017, 2019). Gas contents and isotope geochemistry were studied at different locations over the site. Gas origin was assessed using chemical and stable isotope analyses ($\delta^{13}C$ and δD of C_1 to C_4, $\delta^{13}C$ and $\delta^{18}O$ of CO_2) of the sampled gaseous emissions. The low permeability of thick clays involves that they have the capacity to store the generated gas as free gas, dissolved gas compounds in pore waters and adsorbed gas, the latter providing 20 to 85 % of the total gas in shale reservoirs (Hill and Nelson, 2000). Marine clays that have undergone diagenesis, burial, and finally exhumation are submitted to weathering/oxidizing processes, which result in mineralogical, petrophysical, and chemical changes (Lerouge et al., 2018; Turchyn et al., 2021) and consequently in increasing CO_2/CH_4 degassing (Lerouge et al., 2020). Weathering of carbonaceous shales contributes to ~12 % of the estimated annual CO_2 flux (Jaffe et al., 2002). For this reason, we additionally carried out rock degassing experiments in order to define the chemistry and isotopic composition of the gases fixed in the local soils, surficial weathered shales and shales at ~20–40 cm depth. The extraction of dissolved and sorbed gas from shales remains challenging. Most of desorption experiments in gas-bearing shales and coals are conducted in presence or absence of saturated salt solutions and at varying high temperatures to reduce experimental time (Liu et al., 2016; Ma et al., 2020; Wang et al., 2015), with the risk of inducing secondary processes and poorly constrained isotopic fractionations (Niemann and Whiticar, 2017). Unlike desorption experiments, the degassing experiments we developed on shales from Rochasson were conducted at ambient temperature for a duration defined by the time necessary for reaching a steady state of the gas pressure. Our study demonstrates that rock degassing significantly contributes to our understanding of macro- and micro-seeps in addition and complementary to gas flux measurements.

2. Site context - regional geology and gas seep description

Rochasson is a hydrocarbon gas seep discovered in the 1970s during geological investigations in the French Subalpine Chains at Meylan, near Grenoble, SE France (Debelmas, 1978). The Rochasson site is located on the left side of a thalweg at the top of the "Terres Noires" shales near the contact with overlying limestone. The gas seep is located on the eastern border of the large synclinal structure of the Chartreuse massif that dominates the Isère plain at 1200 m and has a concave shape (Fig. 1). The present-day morphology is due to glacial erosion reworking a structural depression developed along a set of faults parallel to the Belledonne Massif. Two successive cliffs, marking the Massif's summit, allow visualizing the complete series of the Upper Jurassic, which present a general of 20–30° dip to the NW. The first ~100 m high cliff corresponds to Tithonian "Tithonic" limestone, the second ~200 m high cliff to Lower Kimmeridgian – Upper Oxfordian limestone. A wooded area developed on marly limestones (Lower Kimmeridgian) separates the two cliffs. A second wooded area below the cliffs marks the transition to the Upper Oxfordian (locally called Argovian) marly limestones

followed by the Callovian-Oxfordian "Terres Noires" shales at the bottom of the series. Locally the slope reaches 70–80° due to the presence of faults that are visible at the level of the cliffs and overlaps in shales. Old and recent scree largely cover these two latter formations. In the area between Meylan and Rochasson, the surficial formations consist of at least two 3–5 m-thick layers of scree separated by a lacustrine clay loam. The alluvium developed on marly limestone and shales produces weathered materials that can locally evolve into muds. Landslides affect the site, in particular at the top of the shales where the slope remains steep. The slope and clays favour water circulations all along the slope, in particular at the scree/substratum contact.

The "Terres Noires" formation can be divided into a lower unit (Upper Bajocian to Lower Bathonian) of dark grey-black finely laminated marl with a few marly limestone beds and an upper unit (Lower Callovian to Middle Oxfordian) of black, slightly laminated, carbonate-rich marl containing carbonate nodules (Antoine et al., 1995; Artru, 1972; Maquaire et al., 2003). The two units are separated by a hard marker layer (Upper Bathonian and Lower Callovian), which is a brownish clayey limestone (Antoine et al., 1995). The black marls are highly stratified rocks, marked by a fine bedding inherited from their deposition in the Tethyan Subalpine basin, including a detrital and a carbonated phase (Antoine et al., 1995). Their carbonate content, essentially represented by calcite, varies from 20 to 35 vol% (Maquaire et al., 2003). The thickness of the "Terres Noires" formation ranges widely; depending on the location within the basin it can attain e.g. up to 700 m in the Digne area (Olivero and Mattioli, 2008), ~1000 m in the Grenoble area (Barféty et al., 1995), and can even exceed 2000 m in other parts of the basin (Antoine et al., 1995; Artru, 1972).

The basin was related to the opening of the Tethys and the Atlantic, with the deposit of sediments later folded and thrusted during Alpine orogeny. Vitrinite reflectance (R_0 values) measurements in sediments from Upper Jurassic to mid-Jurassic horizons within the SW part of the Subalpine Chains suggest temperatures between 100 and 160 °C assuming a heating duration of up to 10 Ma (Moss, 1992). The level of organic maturity of Mesozoic and Tertiary units in the Chartreuse and Vercors massifs suggest that this part of the Subalpine Chains underwent only shallow burial (Moss, 1992). Microthermometric studies of fluid inclusions in diagenetic quartz crystals, sampled in carbonate concretions of Callovian-Oxfordian marls and shales of SE France, provide evidence of prevailing gas inclusions and rare aqueous inclusions (Guilhaumou et al., 1988). The gaseous part of the fluid inclusions, measured by Raman microprobe, consists dominantly of methane (CH_4)

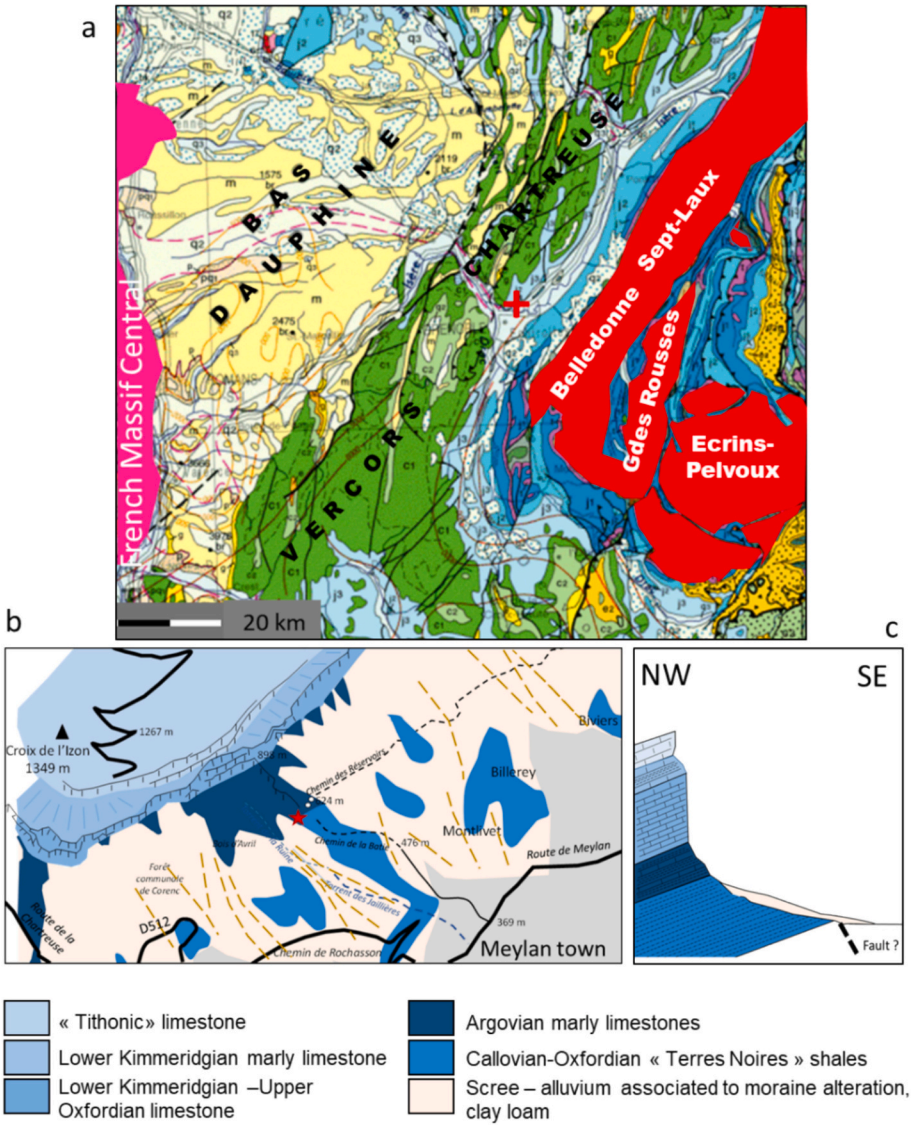

Fig. 1. (a) Geological map with location of the Rochasson site; (b) detail of geology in the area of Rochasson; (c) lithology along the eastern border of the large synclinal structure of the Chartreuse massif.

with various proportions of ethane and propane (C_2H_6, C_3H_8), CO_2, H_2S and N_2 (Guilhaumou et al., 1988, 1996). Combined data of microthermometric measurements of aqueous inclusions associated with gas inclusions in quartz crystals indicate that fluid inclusions with wet gas were trapped at temperatures of ~140–180 °C in the western part of the basin and dry gas trapped at higher temperatures of ~180–230 °C in the eastern part (Guilhaumou et al., 1988, 1996).

Previous investigations at the site of Rochasson have been undertaken for soil gas concentrations and gas flux measurements (Gal et al., 2017, 2019). The main gas vent has a limited surface area (2 × 1 m). The gas composition at the main vent shows slight variations with time; measurements during the last campaign indicate that the dominant gas phase at the main seep is CH_4 (95 %) mixed with C_2H_6 (1.9 %) and traces of CO_2 (0.4 %), N_2 (0.35 %), C_3H_8 (0.3 %), and ^4He (0.007 %) (Gal et al., 2019). The CO_2 monitoring of the surrounding area provides evidence of a strong anomaly at the western part of the site. Overall methane flux at the site, if both the macro-seep and diffuse micro-seepage are considered, is estimated to 4 kg per square meter per day, corresponding an annual emission of ~5 tons of CH_4 at Rochasson (Gal et al., 2019).

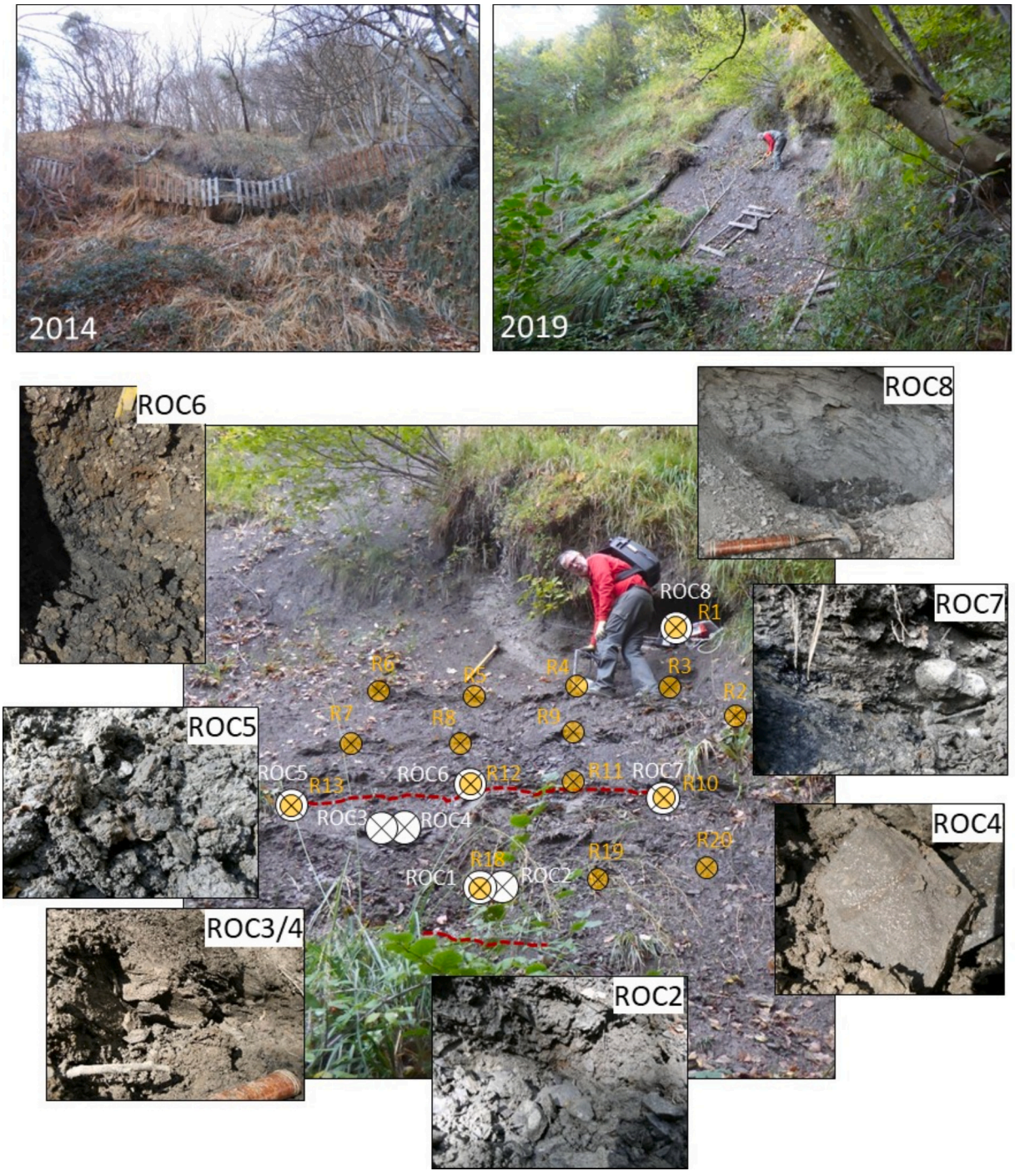

Fig. 2. Photos of the Rochasson site and samples taken during fieldwork. White circles indicate the sampling locations for rock degassing experiments; orange circles indicate points for soil gas flux measurements (further points are located outside the image section).

3. Materials and methods

3.1. Fieldwork and sample conditioning

Reassessment of the site was performed in October 2019. Fieldwork included soil gas flux measurements, gas sampling for concentration analyses and clay sampling for degassing experiments and rock characterization. The area next to the main gas seep has a surface without vegetation and was exposed to atmosphere after a landslide of the clay slope occurred in 2016. A total of 30 points were chosen to measure the gas flux from soil around the main seep, covering an area of 25 m × 10 m (E-W/N-S) plus one remote location (forested area with a distance of 30 m to the south, for a detailed plan and gas flux results refer to Supplementary data Figs. S-1 and S-2). Gas flux data were acquired by using the accumulation chamber technique with external recirculation as described in Gal et al. (2019). Similarly, soil gas concentrations were measured on 10 selected spots identified during the flux measurements, using a LFG20 portable infrared gas analyzer (ADC Gas Analysis Ltd., UK) plugged to a soil gas probe with insertion depths between 10 and 100 cm in the soil. On these 10 measurements, four were collected in IsoTube® containers and stored at room temperature until later analysis.

Clay/shale samples for rock characterization and degassing experiments were taken and conditioned the same day. Eight samples were collected at different points within the area of the gas emission (Fig. 2), and one soil sample within the forest from the same remote location as already described above. Most samples were taken at the surface, except ROC2 (same location as ROC1) and ROC4 (same location as ROC3), which were taken at depths between 20 and 40 cm below the surface. ROC8 is the closest sample to the main vent of the methane emission.

The samples were immediately enclosed in an aluminium foil at the field site in order to minimize contact with atmosphere and avoid water evaporation. The aluminium-wrapped samples were further conditioned the same day. The part of sample, which was destined for water content analyses, and mineral and chemical characterizations, were left in their aluminium-wrapping and then directly conditioned in heat-sealed aluminium flat bags under vacuum. Samples destined for degassing experiments and subsequent gas monitoring were weighed and further conditioned in customized glass jars under a He pressure of ~800 mbar (using a field-lab vacuum-line) following the procedure described in Lerouge et al. (2020).

3.2. Rock characterization

Optical microscopy was carried out on thin polished sections of rock and soil, using an Olympus BH2 microscope with transmitted and reflected light techniques. Water content of the samples that were conditioned in aluminium flat bags was determined by measuring the mass difference before and after lyophilisation. Total carbon content was analysed using a Jobin Yvon EMIE 820V Carbon/Sulfur Analyzer. Organic carbon (TOC) analysis was performed by the same technique after acid treatment of the samples to remove carbonates.

FTIR spectra were acquired on a Bruker Equinox IFS55 spectrometer by transmission through a pellet made of a mixture of 150 mg KBr with about 1 mg of sample. For each spectrum, 32 scans were performed with a frequency range from 4000 to 350 cm^{-1}; the spectral resolution for this study was always 4 cm^{-1}. Spectra were corrected from the background and normalized to pure calcite (Omya) for calcite quantification; peak deconvolution was performed using the software Fityk®.

Four samples (ROC2, ROC3, ROC5 and ROC8), were analysed by Raman spectroscopy of carbonaceous materials (RSCM) in order to evaluate their thermal maturity (Lahfid et al., 2010; Saspiturry et al., 2020); more details on the method are provided in the Supplementary Data). Raman spectral data were obtained by using a Renishaw InVIA™ microspectrometer coupled to a Leica DM2500 microscope. The excitation laser was a Diode Pumped Solid State (DPSS, λ0 = 514.5 nm). In this study, we used an x100 objective (NA = 0.90) to focus the laser beam, all samples were analysed using thin-sections exposed to a power of around 0.5 mW at sample surface. The Raman spectrometer was operated using static scanning mode with large spectral windows from 700 to 2300 cm^{-1}. To check the within-sample structural heterogeneity, at least 10 spectra were recorded for each sample.

3.3. Gas monitoring during rock degassing experiments

The glass jars containing the samples were stored in a room at an almost constant temperature (~20 °C), and regularly monitored for total gas pressure (P_{total} expressed in bar) and concentrations of different gas species (CO_2, alkanes, oxygen and nitrogen) on a Varian star 3400 CX gas chromatograph over several months (at least 2 months). O_2 and N_2 were systematically measured to test the gas-tightness of the glass jars. Concentrations of gas species ($X_{gas\ species}$) are given in volume percent. The uncertainty on the concentrations of CO_2, alkanes, O_2 and N_2 in the gas phase was 3 %. The detection limits for gas concentrations were 0.001 % for CO_2, O_2 and N_2, and 0.0002 % for alkanes. The uncertainty on the total pressure measured in the chromatograph was 3.10^{-3} bar.

The concentrations of gas species ([Gas species]), the total pressure (P_{total}), the sample mass (M), and the gas volume (V_G) in the glass jar allowed estimating the concentrations of gas expressed in mmol/kg of soil-rock, according to the equation (Lerouge et al., 2020):

$$[\text{Gas species}] = \frac{X_{\text{gas species}}}{100} \times P_{\text{total}} \times \left\{ \left(\frac{V_G}{R \times T} \right) \Big/ \left(\frac{M}{1000} \right) + \frac{1}{K_{\text{H(gas species)}}} \right\}$$

For CO_2, the equation takes into account the different dissolved carbonate species:

$$[\text{CO2}] = \frac{X_{\text{CO2}}}{100} \times P_{\text{total}} \times \left\{ \left(\frac{V_G}{R \times T} \right) \Big/ \left(\frac{M}{1000} \right) + \frac{\left(1 + K_1 \times [\text{H}^+] + K_1 \times K_2 \times [\text{H}^+]^2\right)}{K_{\text{H(CO2)}}} \right\}$$

where K_1 is the reaction constant for $CO_2(aq) = H^+ + HCO_3^-$ and K_2 is the reaction constant for $HCO_3^- = H^+ + CO_3^{2-}$ (Giffaut et al., 2014).

CO_2 and hydrocarbon concentrations were regularly measured during 135 days in all the glass jars. The evolution of CO_2 and alkanes concentrations with time provides evidence of different degassing behaviours. An additional gas monitoring of colluvium samples ROC3 and ROC5 and of outcropping shale ROC7 has been carried out for 98 days, to test the capacity of the rock to (re)produce gas and to check if there is a progressive change from CO_2 to CH_4 production due to anoxic conditions we imposed in the glass jars. For that, the gas phase present at the end of the first monitoring phase was pumped out (on a laboratory high vacuum line) and replaced by helium under the same conditions as during the first degassing phase.

3.4. Isotopic analyses

Carbon and oxygen isotopic compositions were determined for bulk calcite in shales, colluvium and soil samples. Calcite was extracted from ~400 mg of clay/shale samples by acid attack with pure phosphoric acid, reaction was performed at 25 °C for 4 h. Produced CO_2 gas from carbonaceous samples obtained in this way were analysed by Isotope Ratio Mass Spectrometry (IRMS) as described below. At the final stage of the degassing experiments (gaseous samples in glass jars), as well as on gas samples from the field (direct emissions sampled in IsoTubes) carbon and oxygen isotopic analyses of CO_2 and carbon and hydrogen isotopic analyses of methane and higher alkanes were performed (analytical methods described hereafter).

3.4.1. Carbon and oxygen isotopes of CO_2

An aliquot of gas of each sample (from calcite preparations, direct gas emissions and/or rock degassing experiments) was transferred into He-flushed Labco®-vials using gas-tight syringes. Specially adapted sampling heads to each gas containing device (including silicone septa) were prepared on a vacuum-line before each sample transfer. The stable carbon isotopic composition of CO_2 ($\delta^{13}C_{CO2}$) was analysed with a continuous flow Thermo Finnigan Delta ^{plus} XP isotope ratio mass spectrometer equipped with a GasBench II (Thermo Finnigan) for gas preparation and introduction. Isotopic compositions are reported in δ units relative to international standards, defined by: $\delta = (R_{Sample} / R_{Standard} - 1) \times 1000$ ‰ where R is the measured isotopic ratio in the

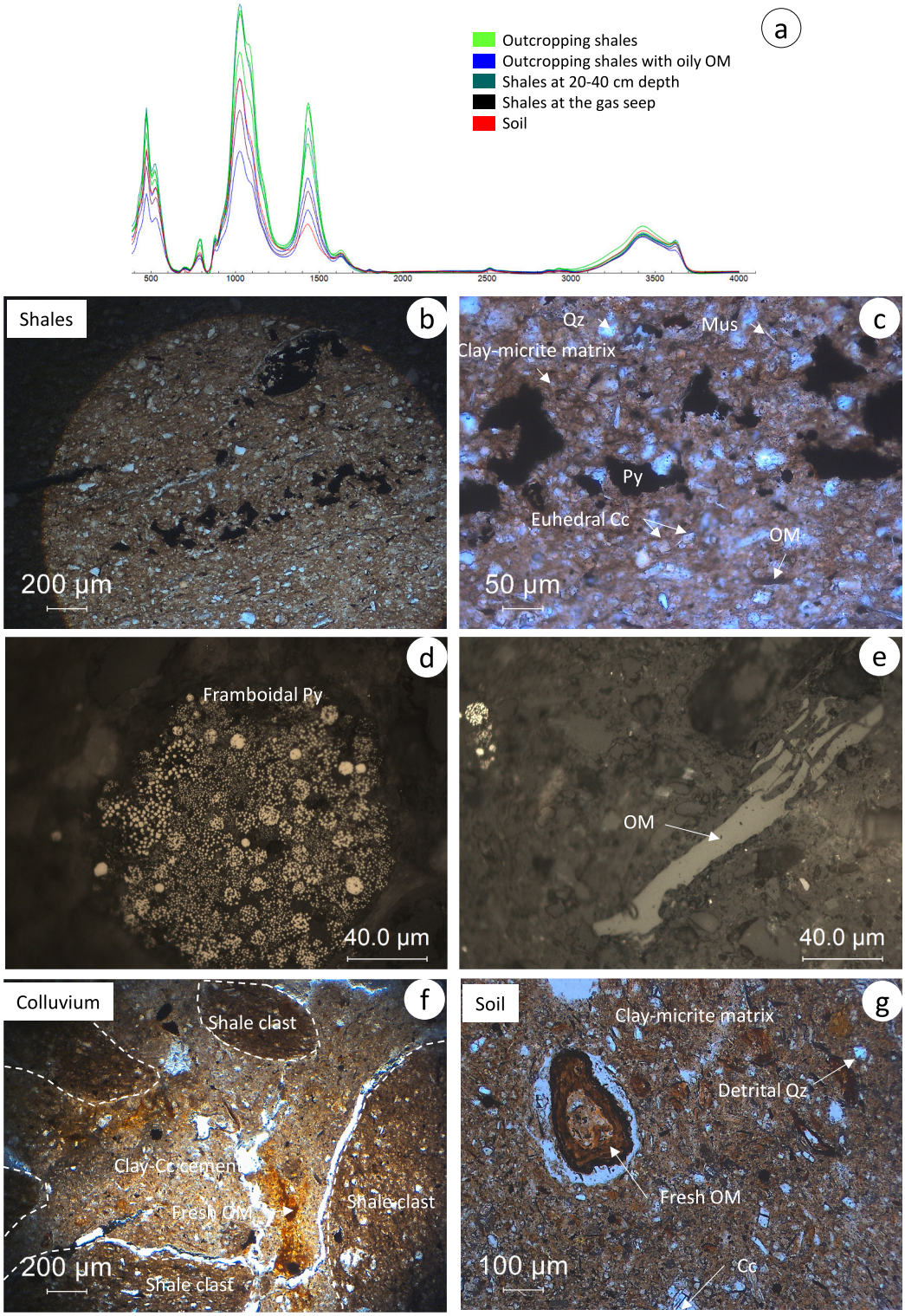

Fig. 3. Infrared spectra of the shales, colluvium and soil (a) and optical microscopic observations of samples – (b) General micrograph of shale at 20–40 cm depth; (c) Detailed mineralogy of shales; (d) framboidal pyrite in shales; (e) Organic matter (OM) in shales; (f) Texture of colluvium; (g) General micrograph of soil showing their texture and mineralogy.

sample and in the standard: Vienna Standard Mean Ocean Water (VSMOW) for oxygen, Vienna Pee Dee Belemnite (VPDB) for carbon. Internal reproducibility was ±0.2 ‰ for oxygen and carbon; accuracy for $\delta^{13}C$ measurements with respect to VPDB standard is better than ±0.5 ‰.

3.4.2. Carbon and hydrogen isotopes of CH_4 and C_{2+} alkanes

Stable carbon and hydrogen isotope compositions of individual hydrocarbon gas compounds ($\delta^{13}C_{C1\text{-}C4}$ and δD_{C1}) were measured by GC/IRMS using a Trace GC Ultra gas chromatograph interfaced to a Delta ^{plus} XP (Thermo Finnigan). The interface was configured with a combustion furnace at 940 °C for carbon, or with a high-temperature furnace at 1420 °C for hydrogen isotope analyses, respectively. Individual hydrocarbon compounds were separated on a PoraPLOT Q column (25 m × 0.32 mm × 10 μm) using a temperature gradient starting at 30 °C for 6 min, subsequently increased at a rate of 15 °C/min to 200 °C. For low concentrations, gaseous hydrocarbons were preconcentrated on a Carbosieve-packed fritted inlet liner for Optic 3 Injectors (ATAS GL Sciences), following the injection method as described by Blessing et al. (2015). Analyses were performed in triplicates, for $\delta^{13}C$ the measurements are represented relative to VPDB and for δD relative to VSMOW. Standard deviations are better than ±0.5 ‰ for carbon and ± 5 ‰ for hydrogen, respectively.

4. Results

4.1. Petrology

Soil and rock samples collected on the outcropping shales of the Rochasson site all consist of a predominant clay-rich fraction associated with detrital quartz grains and carbonates. The carbonate fraction estimated with infrared spectrometry is ranging from 5.4 to 19.4 wt% (Fig. 3). ROC2 and ROC4, sampled between 20 and 40 cm below surface, and ROC8, sampled near the main vent, are hard-bedded and fractured shales. The calcite fraction represents 5.4 to 16 wt% of the rock and includes bioclasts (shells) and diagenetic carbonates (micrite and euhedral calcite). A part of the bioclasts is recrystallized into sparite. Quartz occurs as small-sized detrital grains dispersed in the clay matrix, but also as small lenses cemented by calcite. Pyrite occurs as isolated framboids or clusters of framboids. Oxidation of pyrite remains limited. The total organic carbon (TOC) ranges from 3.7 to 4.8 wt%. Organic matter occurs as detrital particles of various origins that has matured with burial. The water content ranges between 11 and 14 wt%.

ROC1, ROC3 and ROC5 sampled at the surface are plastic and sticky colluvium, which essentially consist of rounded clasts of shales with minor detrital quartz and limestone clasts in a clay- and fine-grained calcite matrix. The total calcite content ranges between 10.4 and 19.4 wt%. Pyrite is present. However, the presence of iron hydroxides and gypsum on the outcrops indicates oxidizing conditions in the colluvium. The TOC varies between 4.5 and 5.4 wt%. Organic matter occurs as detrital particles matured with burial and as fresh particles and roots. The water content of colluvium samples ranges between 20 and 23 wt%. Although ROC6 and ROC7 are sampled at the surface, the rather low oxidation of pyrite suggests relatively well-preserved reducing conditions. These two samples are characterized by a low calcite content (7.1–9.3 wt%) and dark organic matter, dense and oily in aspect (TOC ~4.4–4.9 wt%). The water content (22 wt%) is in the same range as in other outcropping samples. The ROC forest soil, sampled at ~30 m below the gas seep site, is plastic, does not show any residual structure of shale, and consists of an important clay fraction associated with detrital quartz and fine-grained carbonates (~5 wt%). Small roots are abundant. The TOC and the water contents are in the same range than that of colluvium samples, 4.7 and 23 wt%, respectively.

4.2. Isotopic compositions of calcite

The $\delta^{13}C$ values of bulk calcite in shales, colluvium and soil samples are quite similar and range between −0.7 to +0.5 ‰ (Table 1). The calcite $\delta^{18}O$ values in shale, colluvium and soil samples are also quite close and range between +26.9 and +27.6 ‰, except the ROC1 sample, which has a slightly lower calcite $\delta^{18}O$ value of +25.2 ‰. The $\delta^{13}C$ and $\delta^{18}O$ of calcite in claystone is consistent with calcite precipitated from marine-derived fluids. The similarity in isotopic compositions of calcite suggests that calcites present in colluvium and soil are no neoformations but are inherited from marine carbonates without being altered by subsequent isotope exchange reactions.

4.3. RSCM geothermometry

The Raman spectrum of carbonaceous material (CM) is composed of first-order and second order regions. In our work, we recorded Raman spectra only for the first-order region (700–2000 cm^{-1}). The obtained Raman spectra of CM are composed of two broad bands (e.g. (Wopenka and Pasteris, 1993). The relative intensity maxima of these bands (D and G), are ~1350 cm^{-1} and ~1600 cm^{-1}, respectively. The G and D bands are separated by a Raman signal named D3 band located at about 1500 cm^{-1} (Sadezky et al., 2005). The analysis of Raman spectra reveals no prominent variations in the structure of CM measured in this study (Supplementary data Fig. S-3). The shape of Raman spectra indicated a low thermal maturity of the samples analysed. The analysis of these spectra reveals a similarity in all acquired spectra. Based on comparison of the Raman spectrum shape of each sample to the reference series published in Saspiturry et al. (2020), we estimate the qualitative RSCM peak temperature to be 140 °C with an uncertainty of 20 °C.

4.4. Soil gas flux measurements

Gas fluxes were measured on thirty points (R1 to R30) at the site in October 2019 (Supplementary data Figs. S-1, S-2). A CO_2 flux existed on all thirty locations and values ranged from 0.12 to 8.24 (0.0025–0.17 mol) g/m^2/h with a mean value of 2.14 ± 1.73 (0.044–0.03 mol) g/m^2/h. A CH_4 flux was measured on 18 of the 30 measurement locations. The CH_4 flux values ranged from 0.06 to 430 (0 to 26.9 mol) g/m^2/h with a mean value of 58.8 ± 117 g/m^2/h. The value measured at the gas macro-seep (point R1) was 263 g/m^2/h; four high values, ranging between 50 and 430 g/m^2/h, were measured along a line few meters below the gas seep (points R9 to R12). When a CH_4 flux was measured, the gas phase was depleted in oxygen. The maximum depletion was −18.8 g/m^2/h of O_2.

4.5. Soil gas concentrations measured at the field site

Unlike in 2015 (Gal et al., 2017), the soil gas concentrations were not systematically measured in 2019, due to the landslide that has occurred since and the subsequent difficulty to lower the probe to 1 m depth. More specifically, the CO_2 rich zone defined in 2015, affected by the landslide, was not explored again. Therefore, most of the CO_2 concentrations in soil gas were very low in 2019 especially considering the frequent absence of vegetation. Based on these measurements, it was not possible to highlight the occurrence of CH_4 oxidation processes nor to clearly point to respiration processes in the soil. Nonetheless, the low O_2 concentrations measured in the presence of CH_4 may indicate such reactions.

4.6. Molecular and isotopic compositions of gas seep emissions

Four soil gas samples, R1, R4, R5, and R14 were collected in the field for later gas composition and isotopic analyses of CO_2 and alkanes (Table 2). The gas contains an important oxygen and nitrogen contribution from atmosphere. The lowest atmospheric contribution is

Table 1
List of the samples, their main characteristics (sediment type, position, mineralogy), water content, calcite content, calcite $\delta^{13}C$ and $\delta^{18}O$, and total organic carbon (TOC) concentration.

				H_2O	Cc	$\delta^{13}C$	$\delta^{18}O$	TOC
				wt%	wt%	‰ VPDB	‰ VSMOW	wt%
ROC1	Colluvium	Surface	FeOx, roots	23	19.4	−0.7	25.2	5.40
ROC2	Shale	20–40 cm	FeOx, Cc	11	16.0	+0.5	26.9	3.70
ROC3	Colluvium	Surface	FeOx	20	18.4	0.0	27.2	4.55
ROC4	Shale	20–40 cm	FeOx, Cc	11				
ROC5	Colluvium	Surface	FeOx	23	14.6	−0.5	27.6	5.03
ROC6		Surface	MO	22	10.4	0.5	27.6	4.44
ROC7		Surface	MO, nodules	22	7.1			4.86
ROC8	Shale	Main seep		14	9.3	−0.3	27.6	4.75
ROC soil	Soil	Surface	Grass cover	23	5.4	0.2	27.6	4.74

Table 2
Molecular and isotopic composition of the gas collected in IsoTubes; data from precedent campaigns are included for comparison (*concentration data published in Gal et al., 2017, % atm = volume percentage of atmospheric gases N_2 and O_2).

Sampling campaign		2015*			2017	2019			
Gas seep		R1	R18	R27	R1	R1	R4	R5	R14
% atm	vol%	63.4	7.3	89.0	91.5	51.7	94.0	87.6	96.4
% other gases		36.6	92.7	11.0	8.5	48.3	6.0	12.4	3.6
CO_2		1.1	0.4	77.7	1.7	0.4	1.6	0.8	67.4
CH_4		89.9	94.7	1.9	95.9	97.5	96.7	97.3	32.3
C_2H_6	vol% recalculated on the sum of CO_2 and alkanes	1.70	1.92	0.02	2.06	1.79	1.50	1.70	0.25
C_3H_8		0.25	0.30	0.01	0.28	0.29	0.10	0.23	0.05
C_4H_{10}		0.06	0.07	0.00	0.06	0.04	0.03	0.03	0.02
C_5H_{12}		0.00	0.01	0.00	0.01	0.00	0.00	0.00	0.00
$\delta^{13}C_{CO2}$	(‰ VPDB)	−22	−12	−34.9	−21	−7.1	−13.6	−13	−40.1
δD_{CH4}	(‰ VSMOW)	−136	−138	−130	−139	−138	−145	−140	−51
$\delta^{13}C_{CH4}$		−38.6	−36.1	−36	−34.8	−35.1	−44.6	−34.4	−14.7
$\delta^{13}C_{C2H6}$						−29		−28.7	
$\delta^{13}C_{C3H8}$					−22.4	−24		−22.9	
$\delta^{13}C_{C4H10}$	(‰ VPDB)					−21.7			

measured in the sample of the main gas seep (R1). The N_2/O_2 ratio is close to that of atmosphere ($N_2/O_2 \sim 3.7$) at this sampling location, and significantly higher in the other samples. The other part of gases present in the R1, R4 and R5 samples essentially consists of methane mixed with minor amounts of C_{2+} (ethane and higher) alkanes and CO_2. In contrast, the gas in the R14 sample mainly contains CO_2 mixed with methane and higher alkanes. $\delta^{13}C$ values of CO_2 vary between −40.1 and −7.1 ‰. $\delta^{13}C$ values of CH_4 are ranging between −44.6 and −14.7 ‰; δD values of CH_4 range between −145 and −51 ‰. Contrary to methane, $\delta^{13}C$ of higher alkanes (C_2 to C_4) show less variations (with less data available for comparison): −29 to −28.7 ‰ for C_2H_6, −24 to −22.4 ‰ for C_3H_8, and −21.7 ‰ for C_4H_{10}.

4.7. Molecular and isotopic compositions of gases from rock degassing experiments

4.7.1. Gas monitoring phase 1

During degassing of CO_2 from colluvium samples (ROC1, ROC3, ROC5) and ROC soil, the concentration attains an almost steady state after 20 to 40 days, whereas it still slightly increases in shale samples (ROC2, ROC4, ROC6, ROC7) even after 135 days (Fig. 4). CO_2 concentrations at the end of the sample degassing vary significantly but remain all in the same order of magnitude (4.3–11.0 vol%). Converted to mmoles of CO_2 per kg of rock, the lowest CO_2 amounts are measured in shale samples below 20–40 cm, which are relatively well preserved from oxidation (0.32–0.76 mmol/kg in ROC2, ROC4), and in outcropping shales that are rich in dark organic matter (0.90–0.92 mmol/kg in ROC6, ROC7). Higher CO_2 concentrations are measured in colluvium, which shows the most important sign of oxidation (1.8–2.7 mmol/kg in ROC1, ROC3, ROC5) and in ROC soil (3.9 mmol/kg). In contrast, in the shale sample collected close to the gas seep (ROC8) the CO_2 concentration increases rapidly without reaching a steady state. It reaches an anomalously high value of 28.7 vol%, corresponding to a value of 14.0 mmol/kg/135 days (or ~0.1 mmol/kg/day).

Concerning the degassing of hydrocarbons, the C_1-C_6 concentrations are significantly lower than the CO_2 concentrations with alkane/(alkane $+CO_2$) ratios based on vol% ranging between 0.5 and 39.1. The lowest ratios are measured in the shale samples from 20 to 40 cm below the surface (ROC2, ROC4: 0.5–3.3) and in the shale sample close to the gas seep (ROC8: 2.1). The evolutions of alkane concentrations with time are very different from that of CO_2. Methane is the major alkane with $CH_4/(C_2 + C_3)$ ratios of 7–2459 (based on mmol) in all the samples except the shale close to the gas seep (ROC8, high amounts of CO_2). The CH_4 concentration attains an almost steady state between 20 and 40 days in the shale samples below 20–40 cm (ROC2, ROC4), with CH_4 concentrations lower than 0.02 % (or 0.01–0.02 mmol/kg). In other samples, the CH_4 concentrations are significantly higher and still increase even after 135 days. Given in mmoles of CH_4 per kg, the CH_4 amounts range between 0.19 and 0.91 mmol/kg/135 days in colluvium samples (ROC1, ROC3 and ROC5) and between 0.10 and 0.32 mmol/kg/135 days in weathered claystone rich in dark organic matter (ROC6 and ROC7). CH_4 concentration is 0.29 mmol/kg/135 days (or 0.002 mmol/kg/day) at the gas seep (ROC8). The highest CH_4 concentration is measured in ROC soil, with a value reaching 2.5 mmol/kg/135 days (or 0.02 mmol/kg/day). Contrary to methane, the C_{2+} concentrations attain a steady state after 20–40 days (Supplementary data Tables S-1 to S-3). They are at least one order lower than CH_4 concentrations. Converted in mmoles of the CO_2 per kg of rock, the highest C_2H_6 concentrations are measured in shale samples below 20–40 cm, which are relatively preserved from oxidation ($3.9\ 10^{-4}$ - $1.7\ 10^{-3}$ mmol/kg in ROC2, ROC4), and in claystones rich in dark organic matter ($5.9\ 10^{-4}$ - $1.6\ 10^{-3}$ mmol/kg in ROC6, ROC7). The C_{3+} concentrations are lower than C_2H_6

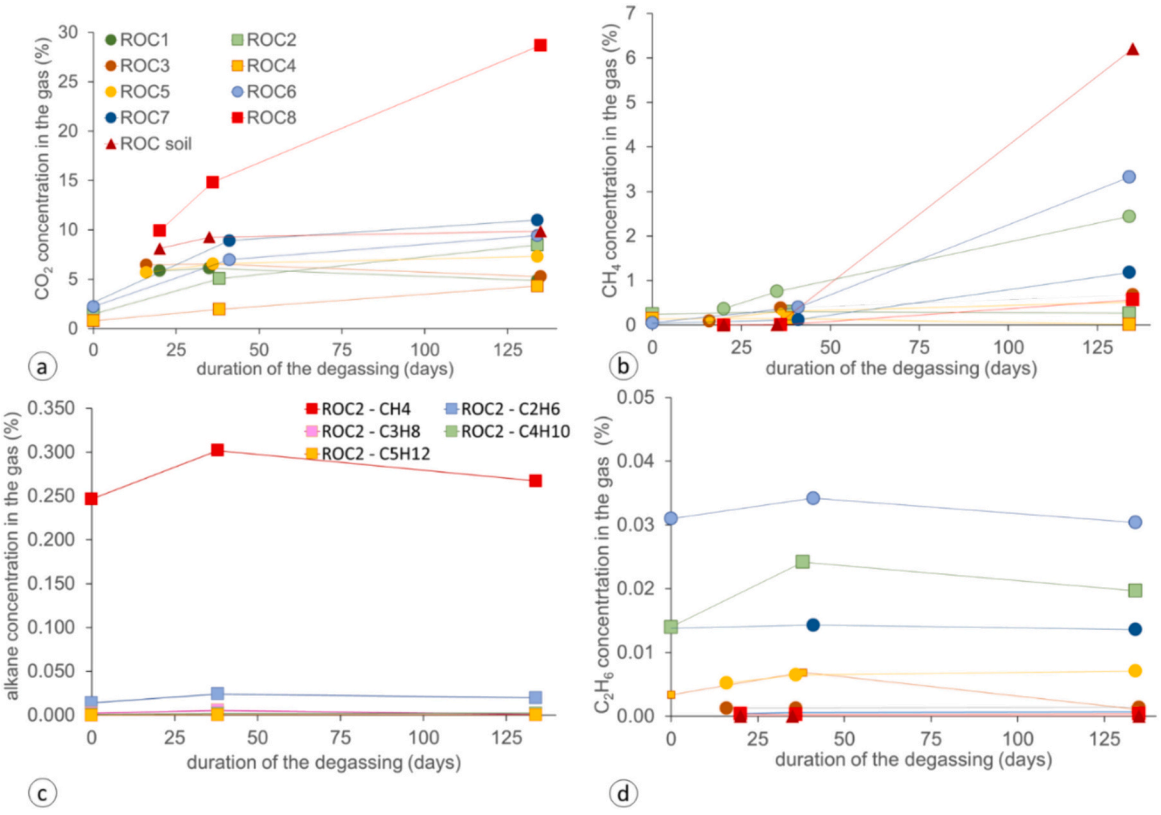

Fig. 4. (a) Evolution of CO_2 concentrations (given in vol%) with time for all the samples; (b) evolution of CH_4 concentrations (vol%) with time for all the samples; (c) evolution of the concentrations of all the alkanes for the weathered sample ROC2; (d) evolution of C_2H_6 concentrations with time for all the samples.

concentrations in these samples. The C_{2+} concentrations of the gas seep emission (ROC 8) are slightly different than in the surrounding rocks with a C_3H_8 concentration (1.1 10^{-3} mmol/kg) higher than that of C_2H_6 (1.0 10^{-4} mmol/kg). The isotopic compositions of CO_2 ($\delta^{13}C$-CO_2), of methane ($\delta^{13}C$-CH_4, δD-CH_4) and of C_2-C_4 alkanes ($\delta^{13}C$-C_{2+}) vary widely in our dataset (Table 3, Fig. 7a). $\delta^{13}C$-CO_2 are between −43.7 and −22.6 ‰; $\delta^{13}C$-CH_4 range between −77.9 and −27.3 ‰. Contrary to methane, $\delta^{13}C$ of higher alkanes (C_2 to C_4) show smaller variations: −26.3 to −25.7 ‰ for C_2H_6, −24.4 to −22.4 ‰ for C_3H_8, and ~−21.7 ‰ for C_4H_{10} (with less data available for comparison).

4.7.2. Gas monitoring phase 2

The CO_2 and CH_4 concentrations increase more rapidly than during the first monitoring (Fig. 5). Contrary to methane, the C_{2+} concentrations attain a steady state after ~30 days. Their behaviour is very similar to that of the first degassing; however, their concentrations are lower than that of the first degassing, except the C_3-C_4 concentrations in the ROC5 sample. It is noteworthy that the $\delta^{13}C$-CO_2 of the second degassing

Table 3
Final measures of total pressure in the glass jars, N2 concentration given in vol%, CO_2 and alkane concentrations given in mmol/kg and isotopic compositions of CO_2 and alkanes.

		ROC1	ROC2	ROC3	ROC4	ROC5	ROC6	ROC7	ROC8	ROC soil
P (mbar)		797	769	775	763	787	809	798	1013	874
N_2 (vol%)		3.4	4.65	1.83	4.93	2.06	7.01	3.66	1.35	1.97
CO_2		1.80	0.76	1.90	0.32	2.70	0.90	0.92	14.00	3.90
CH_4		0.91	0.02	0.24	0.01	0.19	0.32	0.10	0.29	2.50
C_2H_6		2.6E−04	1.8E−03	5.0E−04	8.2E−05	2.6E−03	2.9E−03	1.1E−03	2.0E−04	0
C_3H_8		1.1E−04	8.9E−05	2.9E−04	9.6E−05	1.9E−03	6.7E−05	1.3E−03	1.5E−03	0
C_4H_{10}		7.4E−05	1.9E−04	1.4E−04	4.5E−05	9.9E−04	1.2E−04	5.8E−04	1.1E−03	0
C_5H_{12}	mmol/kg soil	0	3.6E−05	0	1.5E−05	1.8E−04	5.7E−05	1.4E−04	3.0E−04	0
alk/(alk+CO_2) (based on vol%)		33.6	3.3	11.3	0.5	6.8	26.4	10.0	2.1	39.1
$C_1/(C_2 + C_3)$ (based on mmol)		2459	13	304	7	42	108	41	171	–
$\delta^{13}C_{CO2}$ (‰ VPDB)		−36	−30	−43.7	−22.6	−40.7	−32.8	−31.8	−32.8	−29.9
$\delta^{18}O_{CO2}$ (‰ VSMOW)		37.7	37.9	38.2	37.7	36	38.2	37.8	37	37.1
δD_{CH4} (‰ VSMOW)		−275	−78	−245	−77	−241	−312	−270	−201	−319
$\delta^{13}C_{CH4}$		−60.3	−30.6	−77.9	−27.3	−66.3	−60.4	−53.6	−42.2	−52.6
$\delta^{13}C_{C2H6}$	(‰ VPDB)		−25.7				−26.3	−26.2		
$\delta^{13}C_{C3H8}$			−22.4					−24.4		
$\delta^{13}C_{C4H10}$								−21.7		

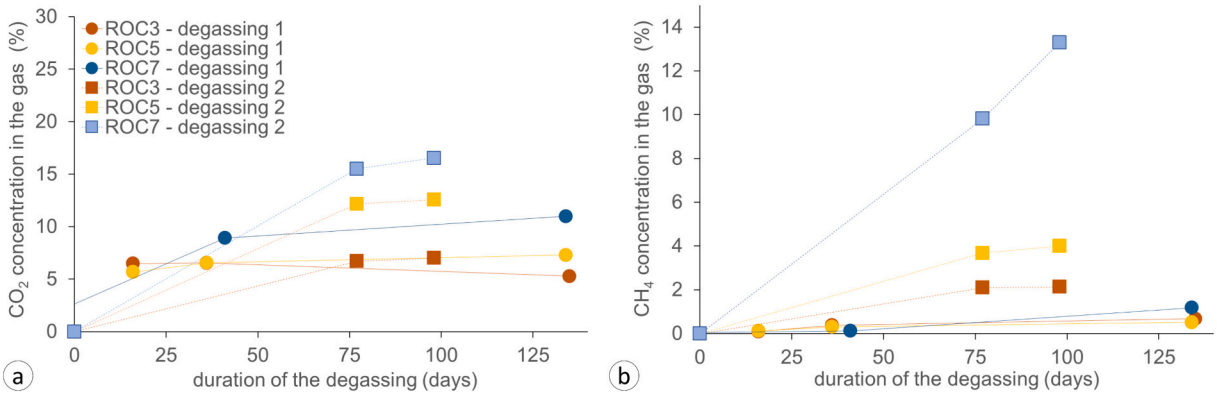

Fig. 5. (a) Evolution of CO_2 concentrations with time of the samples ROC3, ROC5 and ROC7 during the second degassing compared to that obtained during the first degassing; (b) evolution of CH_4 concentrations with time of the samples ROC3, ROC5 and ROC7 during the second degassing compared to that obtained during the first degassing.

of the three ROC samples is very similar to that of the first degassing, while the $\delta^{13}C$-CH_4 is systematically higher, and the δD-CH_4 lower (Table 4).

5. Discussion

5.1. The "Terres Noires" shales at Rochasson

The vegetation cover at the Rochasson gas seep is poor, mainly due to the recent landslide in 2016. The ROC2 and ROC4 shales sampled at 20–40 cm depth show a marl structure with fine platelets characteristic of the "Terres Noires" shales, with a partial loss of cohesion marked by opened bedding. Their mineralogy, including clays, quartz, calcite and framboidal pyrite, and the absence of phase dissolution, are characteristic of an almost preserved reduced marine claystone, and attest of only slight weathering and oxidation (Lerouge et al., 2023, 2018). The layer of colluvium on the surface is thin (<20 cm) and consists mainly of rounded blocks of marl that have locally preserved their structure and mineralogy. The colluvium still contains significant amounts of calcite and residual pyrite, as well as small amounts of iron hydroxides and gypsum, reflecting slow oxidation processes. Observations of the rock structure and mineralogy rather suggest that the landslide was initiated at the limit of the still structured marl, i.e. the lower compact regolith or top of the bedrock, as defined in a weathering profile developed on this type of marl (Bufalo, 1989; Chodzko and Lecompte, 1992; Maquaire et al., 2002). The soil sampled within the forested area with a distance of 30 m to the south ~30 m of the degassing site and outside the zone influenced by the landslide, has a mineralogy similar to that of shale and colluvium, indicating that the soil also developed on shale. However, its calcite content is significantly lower than that of shale, and the absence of bioclasts attest an important calcite dissolution (Lerouge et al., 2018). The difference in calcite content between the soil and the colluvium present in the landslide area near the gas seep confirms that the colluvium corresponds to a very early stage of shale weathering, and that there has been no significant development of soil on the site studied since the landslide. The abundance of organic matter in the "Terres Noires" shales at Rochasson (TOC 3.7–4.8 wt%) is similar to that in other black shales (Petsch et al., 2000). A part of organic matter in colluvium and in soil corresponds to fresh organic matter (mainly roots). Raman spectrometry of organic matter in shale indicates maximum diagenetic temperatures of ~140–150 °C, which corresponds to the temperature range reported for this part of the basin (Guilhaumou et al., 1988; Moss, 1992). This type of organic-rich marine shale is typically enriched in type II kerogen and the main source of petroleum in marine basins able to produce oil or gas at maturation (Tyson, 1987).

Table 4
Carbon and hydrogen isotopic compositions of CO_2 and CH_4, for comparison at the end of the first and the second degassing phase of three ROC samples.

Sample	Degassing phase 1			Degassing phase 2		
	$\delta^{13}C$-CO_2 ‰ VPDB	$\delta^{13}C$-CH_4 ‰ VPDB	δD-CH_4 ‰ VSMOW	$\delta^{13}C$-CO_2 ‰ VPDB	$\delta^{13}C$-CH_4 ‰ VPDB	δD-CH_4 ‰ VSMOW
ROC 3	−43.7	−77.9	−245	−43.7	−60.9	−300
ROC 5	−40.7	−66.3	−241	−40.5	−59.3	−306
ROC 7	−31.8	−53.6	−270	−28.8	−33.8	−287

5.2. The methane macro-seep gas emission at Rochasson

The Rochasson site is a methane macro-seep known for at least 50 years. Debelmas (1978) described these gas emissions as natural gas release, linked to local fractures, over an area of 2–3 m^2 that burned the grasses in the immediate vicinity, sometimes with visible flames occurring, quite similar to the hydrocarbon gas release known as the eternal flames of "Fontaine Ardente" at Le Gua near Vif (Debelmas, 1978). CO_2 is a minor component of the emitted gas. The CH_4 flux value measured in 2019 at the gas seep is 263 g/m^2/h. It is higher than that measured in 2017 (31 g/m^2/h) and in 2015 (180 g/m^2/h), while the O_2 depletions are in the same order of −13 to −12 g/m^2/h. The mean flux value (58 g/m^2/h) measured on some tens of square meters is >10 times higher in 2019 than in 2017. Measuring higher CH_4 flux in 2019 may be related to temporal changes in the gas emission rate which may occur at different time scales including very short ones (Gal et al., 2018). It may also be related to the occurrence of the landslide since then, the influence of climatic conditions and/or the location of the measurement points that were not exactly the same from one campaign to another. Such seepage sites are known to be highly heterogeneous at small scale (e.g. (Hong et al., 2013). The highest methane flux values were measured some meters below the "historical" macro-seep and might represent a methane plume moving from the macro-seep downwards, suggesting that the emission pattern can evolve on a very short time basis.

Gas samples most representative for thermogenic gases are R1, R18, and R5; samples from other locations seem to be affected by secondary alterations (discussed in the processes chapter below). Even though the methane flux has changed slightly over time, the composition of the emitted gas remains homogeneous with a gas dominated by methane (90–98 %) and subordinately C_{2+} hydrocarbons, characterized by $C_1/(C_2 + C_3)$ ratios of ~41–47. For gases sampled at R1, R18 and R5, the low $C_1/(C_2 + C_3)$ ratio, the average isotopic values of methane ($\delta^{13}C$-$CH_4 \sim -36$ ‰; δD-$CH_4 \sim -138$ ‰) and presence of C_2-C_4 alkanes (with $\delta^{13}C$-$C_{2+} \sim -29$ to -22 ‰) are consistent with a thermogenic gas of

marine, type II kerogen source rocks (Schoell, 1980). We hypothesize that this chemical and isotopic homogeneity (measured in the gas in recent years), has been maintained since it was first described almost 50 years ago (Debelmas, 1978), strongly suggesting an important source of methane and continuity of production processes.

5.3. Geochemistry of the "Terres Noires" shale gases at Rochasson

Most of the shale gas data in the literature come from sites of shale gas production; and commercially successful shale plays are among those where most published data are available (Milkov et al., 2020). Most such gases from very productive shale plays are of pure thermogenic origin with rather high maturities. Data from non-productive shales are rare (Lerouge et al., 2015; Prinzhofer et al., 2009; Schovsbo and Nielsen, 2017) and early-mature gases are mostly formed in situ and in relatively small amounts (Milkov et al., 2020). Shale formations with gases of early-mature thermogenic and secondary microbial origin have been reported from naturally fractured shale gas plays that may even show gas compositions of predominantly microbial origin (Curtis, 2002). The biogenic (microbial) and/or thermogenic origins of natural gases are commonly determined using binary genetic diagrams, that combine δ^{13}C-CH_4 with $C_1/(C_2 + C_3)$ ratio, with δD-CH_4 or with δ^{13}C-CO_2 (Bernard et al., 1977; Milkov and Etiope, 2018; Schoell, 1980; Whiticar et al., 1986). Thermogenic gas tends to exhibit $C_1/(C_2 + C_3)$ ratios <100 with δ^{13}C-CH_4 > −50 ‰, whereas pure microbial gas exhibits $C_1/(C_2 + C_3)$ ratios >1000 with δ^{13}C-CH_4 ranging between −70 and −55 ‰. However, various contributions of primary microbial, early-mature thermogenic, and radiolytic gases (Naumenko-Dèzes et al., 2022) as well as secondary microbial alterations (biodegradation, CH_4 oxidation) do complicate this picture and interpretations should not be solely based on genetic field plots (Milkov and Etiope, 2018).

The Rochasson gas macro-seep is located at the top of the "Terres Noires" shales just below the Upper Jurassic limestone, in a wooded and grassy zone where the slope begins to be smooth. Contrary to the macro-seep zone and the surrounding landslide area with outcropping shales, other areas are covered with vegetation growing on clay soils developed on the weathering profile of shales. Gas extracted from soil taken at the remote location (ROC soil) initially consists of CO_2, followed by CH_4 degassing when the CO_2 emission ceases (Fig. 6); higher alkanes are absent. CO_2 extracted from soil corresponds to inorganic carbon dissolved (DIC) in pore waters. The DIC of ~3.9 mmol/kg soil or 1.7 mmol/L PW (of pore waters calculated at saturation) is quite low for soil. The δ^{13}C-CO_2 of ~ −30 ‰ points to a microbial origin, due to degradation of (fresh) organic matter according to the aerobic respiration reaction: $CH_2O + O_2 \rightarrow CO_2 + H_2O$, as elsewhere described in soils that have developed on clays (Lerouge et al., 2020). The δ^{13}C-CH_4 (−53 ‰) and δD-CH_4 (−319 ‰) are well comparable to that of freshwater microbial methane indicating acetoclastic methanogenesis (Whiticar et al., 1986; Fig. 7a).

Direct outcrops of shales and overlying clay colluvium are located next to the macro-seep and in the area where soil has not developed since the landslide. Gas principally consists of CO_2, some CH_4 and systematic small amounts of C_{2+} alkanes. The CO_2 concentrations measured in shales at 20–40 cm depth (0.2–0.5 mmol/L PW), in outcropping shales (0.4 mmol/L PW) and in colluvium (0.8–1.2 mmol/L PW) are lower than in soil; overall they increase with weathering intensity. These low concentrations of DIC compared to similar contexts within clays (Lerouge et al., 2020) rather suggest dilution with meteoric fluids and only minor influence of weathering and oxidation on the shales and shale clasts in colluvium that are exposed to the surface since 2016 at the Rochasson site. The δ^{13}C-CO_2 values (~ −30 to −22 ‰) of shale sample gases are very similar to that of soil. This range of values

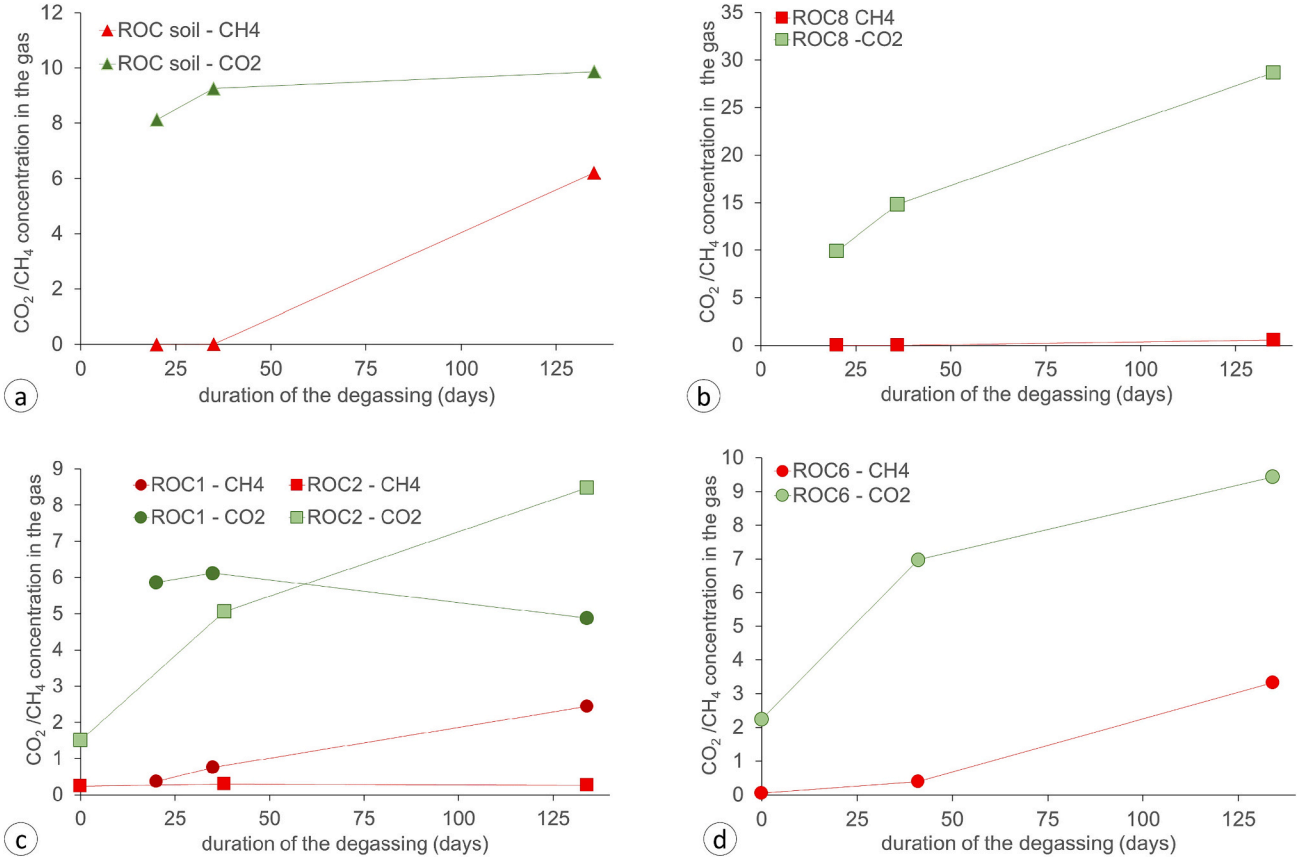

Fig. 6. Monitoring of CO_2 and CH_4 concentrations (given in vol%) with time (in days) – (a) soil developed on shales (ROC soil); (b) shales at the gas seep site (ROC8); (c) colluvium (ROC1) and shales at 20–40 cm depth (ROC2); (d) shales at surface rich in oily organic matter (ROC6).

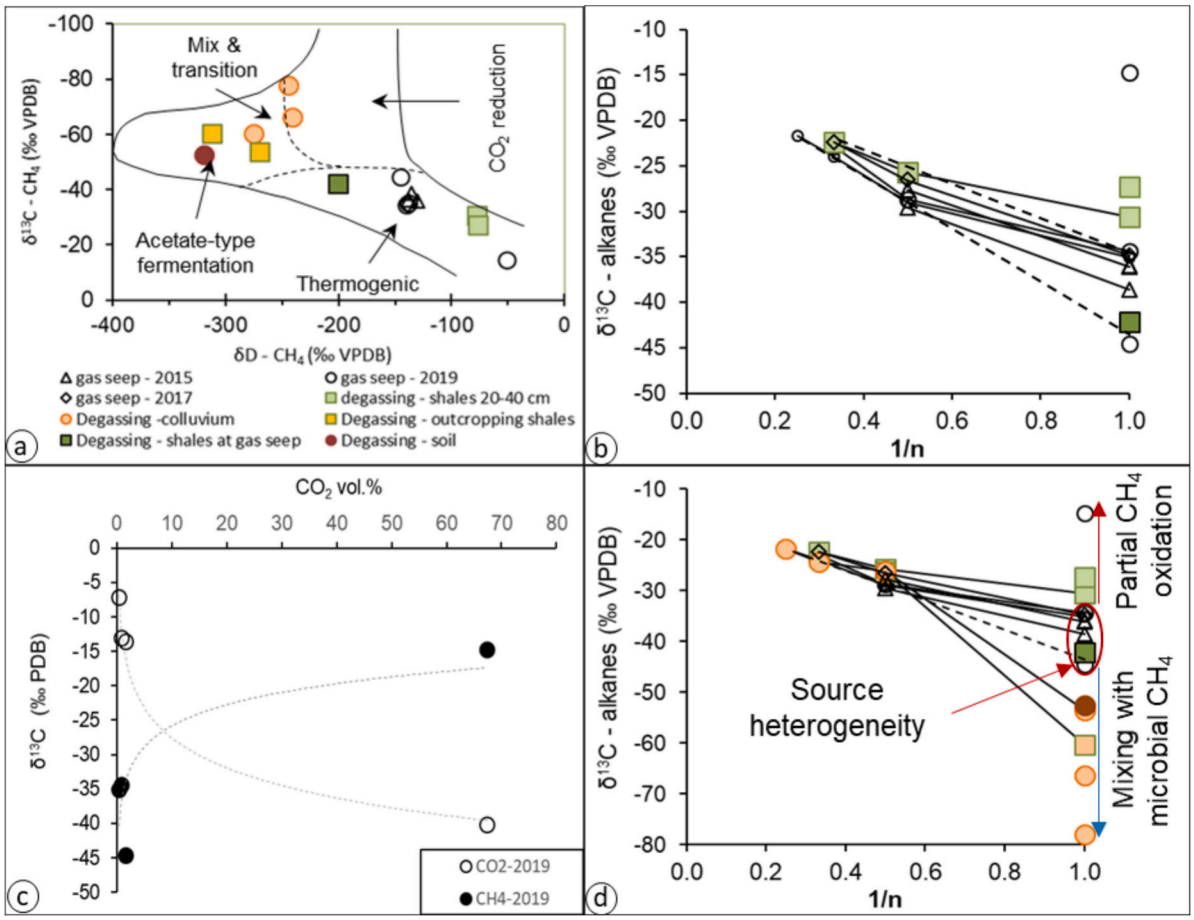

Fig. 7. (a) δD-CH_4 - $\delta^{13}C$-CH_4 diagram of Whiticar et al. (1986) in which are plotted the samples of gas seep and of rock degassing; (b) $\delta^{13}C$ of alkanes in function of the 1/n (n being the carbon number of the gas molecule), in which are reported data from gas seep and gas issue from the degassing of the most preserved shales (20–40 cm) and shale at the gas seep (Chung diagram, 1988); (c) $\delta^{13}C$-CH_4 and $\delta^{13}C$-CO_2 in function of the amount of CO_2 in gas seeps (macro-seep and diffuse micro seepage) measured during the 2019 field campaign; (d) Chung diagram with all the data.

suggests that DIC in shales and colluvium also dominantly results from degradation of fresh OM and is clearly not at isotopic equilibrium with carbonates ($\delta^{13}C \sim 0$ ‰) present in shales. The $\delta^{13}C$-CO_2 values in colluvium (~ −44 to −36 ‰) are lower than in soils and shales, suggesting biodegradation of a ^{13}C-depleted organic matter such as kerogen/oil present in shale clasts of the colluvium (Clayton et al., 1997; James and Burns, 1984; Pallasser, 2000). Unlike in soil gas, small amounts of C_{2+} alkanes are detected in the gas dissolved in pore waters of shales and colluvium (Table 3). During degassing, the C_{2+} concentration rapidly reaches a steady state (Supplementary data Tables S1–S3), indicating that the C_{2+} alkanes are at thermodynamic equilibrium with pore waters and rock (Lerouge et al., 2015). The $\delta^{13}C$-C_{2+}, ranging between ~ −26 and − 22 ‰ are almost homogeneous (measurable only in shale samples ROC2, ROC6 and ROC7), and comparable to the isotopic signatures of the macro-seep gas.

While the C_{2+} hydrocarbons show a similar degassing behaviour, methane degassing, $C_1/C_2 + C_3$ ratios, and methane isotopic signatures are different in shales at 20–40 cm depth, outcropping shales, and in colluvium (Table 3, Fig. 7). In shales at 20–40 cm depth (ROC2 and ROC4) that are, by their visual aspect, considered as the least weathered "Terres Noires" shales, the CH_4 concentration rapidly reaches a steady state (~0.02 mmol/kg), comparable to C_{2+} alkanes, rather indicating a thermodynamic equilibrium for methane in these samples (Fig. 6b). Low $C_1/C_2 + C_3$ ratios (7–13) and the slightly enriched isotopic signatures of methane ($\delta^{13}C$-CH_4 −31/−27 ‰ and δD-CH_4 −78/−77 ‰) indicate that methane is initially of thermogenic origin, comparable to C_{2+} alkanes, but suffered oxidation processes causing isotopic enrichment in methane (Cadieux et al., 2016; Coleman et al., 1981; Rasigraf et al., 2012). Direct comparison of $C_1/C_2 + C_3$ ratios with gaseous emissions at the field (macro-seep and micro seepage) is complicated by the fact that secondary alteration processes and gas migration in the subsurface impact the initial isotope composition and the $C_1/C_2 + C_3$ ratio, respectively (Milkov and Etiope, 2018). The isotopic enrichment in ^{13}C and D of methane within these two shale samples can be compared to $\delta^{13}C$-CH_4 and δD-CH_4 from the direct gas seep point R14, suggesting secondary processes of methane oxidation in the subsurface. In outcropping shales in direct vicinity to the macro-seep point R1 (ROC8) and closeby (ROC6, ROC7), as well as in colluvium (ROC1, ROC3, ROC5), the CH_4 degassing curves increase compared to those of sub-surface shales (ROC2, ROC4) and do not reach a steady state (Fig. 6c). The increase of the $C_1/(C_2 + C_3)$ ratio (41–2459) and the large range of depleted isotopic signatures of methane ($\delta^{13}C$-CH_4: −78/−42 ‰, δD-CH_4: −312/−201 ‰) compared to the macro-seep R1 provide evidence of mixing between thermogenic alkanes and a ^{13}C- and D-depleted methane component (Fig. 7). The $\delta^{13}C$-CH_4, and δD-CH_4 ratios as low as −78 ‰ and −312 ‰, respectively, strongly suggest a methane source with microbial origin (Schoell, 1980; Whiticar, 1999) due to methanogenic microbial activity in surface-near shales where either fresh or detrital OM are biodegraded. Slightly ^{13}C-enriched ethane in shale samples ROC2, ROC6, and ROC7 ($\delta^{13}C$-C_2H_6: −26 ‰) compared to direct gaseous emissions at R1 and R5 ($\delta^{13}C$-C_2H_6: −29 ‰) hints to biodegradation of gas components producing secondary CH_4 with a microbial signature leading to a $\delta^{13}C$-CH_4 as low as −78 ‰. This may indicate the presence of ethane-specific degrading bacteria with a greater isotopic effect on ethane rather than propane (Clayton

et al., 1997; Gong et al., 2017). In our long-term degassing experiments on ROC3, ROC5 and ROC7 we intended to get more indications on ongoing methanogenesis reactions. However, the "reset" to zero under closed conditions resulted in limited access to water (only porewater left in ROC3/5, while ROC7 was completely dry) and strictly anaerobic conditions (no O_2 left) after the second "pumping". The change in CH_4 isotopic compositions we observed indicate shifting reactions from initially CO_2 reduction pathway to more fermentation-like reactions. Different bacterial strains are present at the same time, but active/inactive depending on the prevailing conditions at the time of sampling. As we induced a closed system where nutrients are limited, the relation of δD-CH_4 and H_2O for microbial methanogenesis during degassing phase 2 is not comparable to reactions in natural environments where ~40 % of the hydrogen involved is derived from H_2O during microbial methanogenesis (Schoell, 1980).

In order to go further in the interpretation of hydrocarbons, data are reported in a natural gas plot or "Chung diagram" which enables to differentiate natural gas sources and to visualize the effects of maturation and other post-genetic secondary processes on isotopic distributions in $\delta^{13}C$ of C_1-C_5 alkanes (Chung et al., 1988). If we consider that all C_1-C_5 alkanes are thermogenic and result from the thermal cracking of isotopically homogeneous parent molecules, a sublinear relationship between the carbon isotopic ratios and the inverse carbon numbers of molecules should be observed (Chung et al., 1988). Based on this theoretical relation (non-altered gaseous emission based on $\delta^{13}C$-C_{2+} of R1 and $\delta^{13}C$-CH_4 of R4 and ROC8 as best-fitting representatives of the original thermogenic gas) in the "Chung diagram" (dashed line in Fig. 7d) and the nomogram proposed by Dzou and Milkov (2011), we can estimate a degree of thermal stress at ~150 °C. All samples of the direct emissions at the field site (except R14) and one of the shales sampled next to the main seep (ROC8) show a quite narrow $\delta^{13}C$-C_1-C_4 range within the two dotted lines illustrated in Fig. 7b. Observed slope variations between C_2 and C_3 might be due to heterogeneities of parent molecules and/or slightly increasing maturities. The relatively small δD-CH_4 variations of the macro-seep gases are consistent with this hypothesis. The direct emission at point R14 shows significantly enriched $\delta^{13}C$ and δD values of CH_4 (even > $\delta^{13}C$-C_{2+} of all points available in our data set). This methane anomaly, only a few meters away from the main seep, is associated with a higher concentration of ^{13}C-depleted CO_2, suggesting an important oxidation process of methane (Fig. 7c). A similar hypothesis can be considered for the ^{13}C- and D-enrichment of the δD-CH_4 of ROC2 and ROC4, with either a smaller degree of methane oxidation or slightly different fractionation factors of the oxidation reactions involved. An overview on isotope enrichment factors for aerobic and anaerobic methane oxidation is provided in Rasigraf et al. (2012). Preliminary results of a microbiological study performed at the site show an increased abundance of methanotrophs in Rochasson soil (communicated by (Bott et al., 2020), indicating AOM reactions in zones with a high and continuous CH_4-flow. In natural settings, both, aerobic and anaerobic methanotrophs can be found having niches even in greater depths (Kietäväinen and Purkamo, 2015).

To summarize, methane and C_{2+} alkane concentrations measured at the surface in the area surrounding the macro-seep are highly diluted by CO_2 from different sources. Similar to most of the seep gases they have a thermogenic origin in the "Terres Noires" shales sampled at 20–40 cm depth. Methane, although plotting close to methane of the macro-seep, shows signs of isotopic enrichment due to oxidation processes, thus plots in the upper part of the "Chung diagram". Methane in more exposed, weathered shales and colluvium has a mixed thermogenic and microbial origin and plots in the lower part of the "Chung diagram" (Fig. 7d). Our data are consistent with a behaviour typical for secondary altered thermogenic gases with secondary microbial CH_4 production from degradation of fresh OM and HCs (methanogenesis). It should be noted that microbial methane in weathered shales and colluvium was produced later than CO_2 during degassing, similar to the behaviour in the soil sample. Rock degassing is consequently efficient to extract natural thermogenic hydrocarbons dissolved in pore waters and sorbed on sediment without experimental fractionation, but the anaerobic conditions of the degassing and its duration favour the development of microbial methane production, which does not exist or not significantly enough to be monitored during field acquisitions. This experiment demonstrates that soil, colluvium and weathered shales essentially degas CO_2 at the interface with atmosphere (considered as infinite oxygen reservoir), while they potentially degas CH_4 when oxygen availability at depth becomes limited. This can rapidly be the case in a soil profile developed on low-permeable shales during humid periods (Topp and Pattey, 1997), oxygen diffusion being lower in pore waters than in the gas phase (Bolton et al., 2006). The observed gas evolution during our experiments also indicates that different microbial populations coexist in soil that are involved in CH_4 production by methanogenesis and CH_4 consumption through aerobic and/or anaerobic CH_4 oxidation.

5.4. Timeline/summary of CO_2, CH_4 and C_{2+} production in the "Terres Noires" shales

As seen above, only C_{2+} characteristics of the macro-seep and the "Terres Noires" shales at Rochasson are common, typical for emissions of thermogenic hydrocarbons. The large range of methane and carbon dioxide concentrations and isotopic signatures of seep gases and shale gas provide evidence of complex processes that control gas emissions in outcropping shales. This part of the discussion proposes a scheme to reconstruct the successive processes of OM degradation during diagenesis from sediment deposition and compaction, burial diagenesis, uplift and finally outcropping with exhumation and weathering. A schematic burial curve is shown in Fig. 8, illustrating the evolution of different gases produced within the shale's life history.

Early diagenesis involves deposition and compaction of marine organic-rich sediments. The carbon-rich "Terres Noires" black shales were deposited in a deep marine environment. Marine OM is often described as $C_{106}H_{263}N_{16}O_{110}P$ (Redfield et al., 1963), and more recently with a revised composition as $C_{106}H_{175}N_{16}O_{42}P$ (Anderson, 1995). The former is often reformulated as $(CH_2O)_{106}(NH_3)_{16}H_3PO_4$, both can be simplified as $C_6H_{12}O_6$. In our work, we present general reaction schemes as proposed by LaRowe and Van Cappellen (2011); complete equations can be found elsewhere in the literature, e.g. (Chen and Wang, 1999; Turchyn et al., 2021).

(1) Aerobic respiration: $C_6H_{12}O_6 + 6\ O_2 \rightarrow 6HCO_3^- + 6\ H^+$
(2) Nitrate reduction (NO_3- reduction): $C_6H_{12}O_6 + 24\ NO_3^- \rightarrow 6H^+ + 30\ HCO_3^- + 12\ N_2 + 12\ H_2O$
(3) Manganese (Mn-ox) reduction and Iron (Fe-ox) reduction: $C_6H_{12}O_6 + 12\ MnO_2 + 18H^+ \rightarrow 6\ HCO_3^- + 12\ Mn^{2+} + 12\ H_2O$ and $C_6H_{12}O_6 + 24\ FeOOH + 42H^+ \rightarrow 6\ HCO_3^- + 24\ Fe^{2+} + 36\ H_2O$
(4) Bacterial sulfate reduction (BSR): $C_6H_{12}O_6 + 3\ SO_4^{2-} \rightarrow 6\ HCO_3^- + 3HS^- + 3\ H^+$
(5) Organic matter fermentation → microbial methane: $C_6H_{12}O_6 + 3H_2O \rightarrow 3\ CH_4 + 3\ HCO_3^- + 3\ H^+$
   (a) hydrogenotrophic methanogenesis: $CO_2 + CH_4 \rightarrow CH_4 + H_2O$
   (b) acetoclastic methanogenesis: $CH_3COOH \rightarrow CO_2 + CH_4$
   (c) methylotrophic methanogenesis: $CH_3OH \rightarrow CH_4 + CO_2 + H_2O$
(6) Anaerobic CH_4 oxidation (AOM): $CH_4 + SO_4^{2-} \rightarrow HCO_3^- + HS^- + H_2O$

In the first few centimeters of burial, OM degradation in the ocean and surface sediments is dominated by aerobic respiration (reaction 1), producing mainly CO_2. When oxygen and nitrate (reaction 2) as most efficient oxidants are consumed, redox reactions during early diagenesis such as reduction of manganese or iron oxyhydroxides take over (reaction 3). At deeper burial depths, the anaerobic digestion of OM includes microbial sulfate reduction (BSR, reaction 4), which, due to the high sulfate (SO_4) concentration in seawater, is relatively dominant in marine

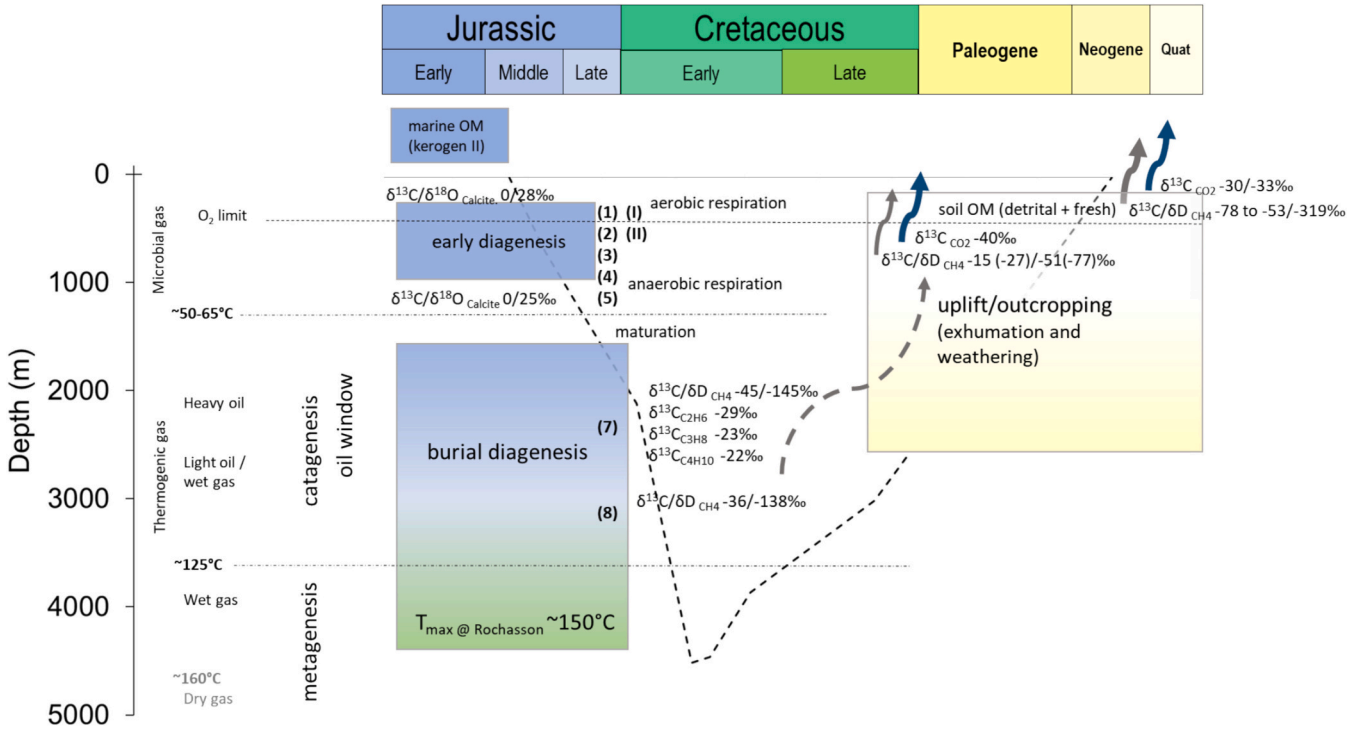

Fig. 8. Schematic illustration of the stages and evolutionary history of the "Terres Noires" shales and its gaseous emissions at Rochasson. Reactional processes are given in brackets and detailed in the main text.

environments. When SO_4 concentrations become rate limiting, remaining organic carbon is fermented by methanogenesis producing CH_4-rich microbial gas (reaction 5). Organic matter fermentation produces acetate and molecular hydrogen, both stimulating methanogenesis (reactions 5a-b). Although acetotrophic and hydrogenotrophic methanogenic pathways can both occur in marine sediments, the hydrogenotrophic pathway is thought to be more important (Whiticar, 1999). Recent microbial studies however, suggest that acetoclastic as well as methylotrophic methanogenesis (utilizing a range of noncompetitive methylated substrates; reaction 5c) may also play a possible role in some coal and shale gas systems (Vinson et al., 2017). This series of reactions, driven by anaerobic degradation of organic matter enhances the release of alkalinity, increase the carbon dioxide (CO_2) buffering capacity of seawater and therefore oceanic CO_2 uptake (Gustafsson et al., 2019). Methane is less dense than pore waters; it migrates through the sediments towards the surface and can be anaerobically oxidized by sulfates to produce DIC and hydrogen sulfide within the sulfate-methane transition zone (SMTZ) (reaction 6).

Pathways such as sulfate reduction, acetate fermentation (reactions 4–5) and methanotrophic reactions (anaerobic methane oxidation, reaction 6) alike produce bicarbonate ions that are precipitating as carbonates. The product bicarbonate inherits its ^{13}C-depleted isotope composition from either organic matter or methane that was involved in the reaction (Loyd and Smirnoff, 2022). The ocean acts as a trap of atmospheric carbon dioxide through the reaction of dissolved carbon dioxide with water to form carbonic acid, bicarbonate and carbonate ions whose concentrations are governed by the carbonate equilibrium system (Middelburg et al., 2020). In such marine environments, diagenetic calcite and framboidal pyrite precipitate from subseafloor production of DIC and hydrogen sulfide, as a result of microbial respiration of organic carbon in the absence of oxygen (Amiel et al., 2020; Turchyn et al., 2021).

Diagenetic minerals in shales at Rochasson are essentially calcite with minor framboidal pyrite. The $\delta^{13}C$ and $\delta^{18}O$ of bulk calcite in these shales are characteristic of calcite precipitated at equilibrium with marine-derived pore waters in shales once mineral saturation attained. The $\delta^{18}O$ of bulk calcite of ~27–28 ‰ rather suggests that most of the calcite present in these shales precipitated at temperatures close to 30 °C during early diagenesis, using the calcite-H_2O oxygen isotopic fractionation of Kim and O'Neil (1997). We found barite nodules in the stratigraphic layer just above the shales, quite typical when $BaSO_4$ precipitates within or close to the SMTZ (Arndt et al., 2009). Within this zone produced methane may be anaerobically oxidized (sulfate-driven AOM, reaction 6) involving anaerobic methanotrophs and sulfate-reducers, typically leading to methane-derived carbonates (=^{13}C-depleted calcites, which we did not observe at our site). We suppose that the ^{13}C-depleted carbonates might be present in the nodules that we observed above the shales (but did not include in our analyses). CH_4 values at some emission zones are significantly ^{13}C-enriched, and may hint to AOM conserved in shale pores, reflecting processes during burial diagenesis. Slightly negative calcite values might hint to an addition of a small fraction of authigenic carbonate that has been produced by AOM processes within the SMTZ to the $\delta^{13}C$ composition of bulk calcites. However, it is much more likely that most of these ^{13}C-enriched CH_4 gas emissions are related to more-recent events, aerobic or anerobic methane oxidation as secondary processes during weathering (see below).

The boundary between early and burial diagenesis is gradational from ~800 to 2600 m below water/sediment interface (Rimstidt et al., 2017), marked also by a gradual cease of microbial activity and increasing rates of thermocatalytic processes (60–80 °C; (Machel, 2001), at this stage essentially all of the organic matter has been converted to kerogen. The transition from biotic to abiotic diagenesis is not only driven by temperature, but also by compaction of the sediment, which inhibits the movement of bacterial cells by reduction of porosity and pore sizes and decreases the diffusion rate of nutriments (Lerouge et al., 2011). Organic-rich shales have a high production and storage capacity for thermogenic gas occurring as free gas, dissolved gas compounds in pore waters and adsorbed gas (Hill and Nelson, 2000). Catagenesis reactions break down kerogen releasing mobile hydrocarbons over the temperature range of the oil window (~60–65 °C to 150 °C; (Stolper et al., 2014). In most sedimentary basins, the onset of petroleum

generation begins at ~50 °C (at depths >1 km, sulfur-rich kerogens generate oil at lower thermal stress than sulfur-poor kerogens; (Seewald, 2003). Within the mesodiagenesis zone at maximum burial the following thermochemical reactions can occur.

(7) Catagenesis (thermal decarboxylation) ➔ thermogenic methane (stepwise reactions leading to n-alkanes (CH_4/C2+) + CO_2
(8) Thermochemical sulfate reduction (TSR methane oxidation): $CaSO_4$ + hydrocarbons (C1–5) ➔ $CaCO_3 + H_2S + H_2O \pm S \pm CO_2$

In the case of Rochasson, burial depths reached temperatures at the high temperature end of the oil window where catagenesis reactions produce wet gas (C2+ -rich). The isotopic compositions of Rochasson seep gas samples not affected by secondary alterations, i.e. the most representative for thermogenic gas samples (R1, R18, R5), are characterized by δ^{13}C-$CH_4 = -36 \pm 2$ ‰, δD-$CH_4 = -138 \pm 2$ ‰ and δ^{13}C of C2 to C4 from −29 to −22 ‰. Our isotopic data and Raman spectrometry on OM in "Terres Noires" shales, as presented above, inform on a maximum temperature of 150 °C attained by OM during burial. Chemical oxidative processes (TSR, thermochemical sulfate reduction, reaction 8) can be an important reaction in hydrocarbon-containing reservoirs with earlier oil, wet gas, and later methane-dominated dry gas stages (Cai et al., 2022). TSR is commonly observed in carbonate reservoirs, the estimated minimum temperatures required for TSR are between 120 and 140 °C (Seewald, 2003) and 100–140 °C (Machel, 2001). We have not observed any indications for TSR reactions at our site. At even higher temperatures, catagenesis transitions into metagenesis generating only CH_4 (dry gas; this stage has clearly not been reached at Rochasson).

The exhumation stage during uplift is mainly accompanied by physical processes such as confining pressure relief, increasing permeability, shrinking in the horizontal direction with creation of vertical fractures. Shales with high quartz, feldspar and carbonate content are brittle and thus prone to weathering processes in the critical zone. Interactions of reduced shales with atmosphere and surficial waters result in mineralogical, petrophysical, and chemical changes (Lerouge et al., 2018; Turchyn et al., 2021), but also in secondary alterations of shale gas molecular compositions and C- and H- isotope ratios. These interactions are largely driven by biological activity, of macro- and microorganisms, including vegetation. Major mineralogical/chemical changes include pyrite oxidation, carbonate dissolution and OM /kerogen/oil degradation associated with slight pH decrease and alkalinity/DIC and DOC increase (Lerouge et al., 2018).

At depths where groundwater can penetrate the shales, swelling increases pore pressure, leading to the release of hydrocarbon gas, which, combined with other factors that increase the local permeability, creates the conditions for gas emissions to the surface (Rimstidt et al., 2017). Microbial methane produced in these freshwater penetration zones from in-situ biodegradation in shales (following the same methanogenesis pathways earlier discussed) will mix with gas of thermogenic origin. Chemical weathering starts with the infiltration of surface and groundwaters containing dissolved CO_2 and O_2 to various depths below the surface. Dissolution of carbonate minerals can dilute the methanogenic signal in DIC and in the gas-phase CO_2. Secondary alterations such as biodegradation of oil and/or natural gas components as well as microbial oxidation of CH_4 in sediments/soils/soil water modify isotope ratios. Previous work has shown differences in the susceptibility of C_{2+} components to biodegradation; often propane (C_3) seems to be selectively consumed at first; the debate of which compound is most prone to bacterial degradation is ongoing (Gong et al., 2017). At Rochasson, we observed biodegradation of C_{2+} gas components producing secondary CH_4 with a microbial signature due to rather ethane-specific bacteria. In terms of oxidation processes, methane is the most reactive, with two major reactional pathways.

(i) Aerobic oxidation: $CH_4 + O_2 \rightarrow CO_2 + H_2O$
(ii) Anaerobic oxidation: $CH_4 + SO_4^{2-} \rightarrow HCO_3^- + HS^- + H_2O$

Aerobic conditions occur in colluvium and shales in direct contact with atmosphere and in the first few meters of shales where oxygen diffuses. Fresh breaches with only slight mineralogical changes as we could observe after the landslide in 2016, suggest that the oxygen diffusion zone in the area was relatively limited. Anaerobic conditions correspond to the zone where oxygen is not present, but where sulfates diffuse in pore waters.

In the δ^{13}C values of C_2-C_4 of samples with concentrations sufficient for isotopic measurements, we found no indications of secondary alterations. In several cases (direct gaseous emissions and in shales) we observed enriched CH_4 isotopic ratios indicating active oxidation reactions; microorganisms involved in oxidizing methane produce higher CO_2 flux at the surface above these soils. In most of our shale samples, δ^{13}C values of CH_4 are depleted indicating significant input of microbial methane due to different methanogenic pathways.

Calcite dissolution (δ^{13}C-CO_2 of ~ −10 ‰), OM /kerogen/oil degradation (δ^{13}C-CO_2 ~ −33/−30 ‰) and methane oxidation (δ^{13}C-CO_2 of ~ −43/−36 ‰) contribute to the increase of CO_2 degassing and of DIC and are characterized by different δ^{13}C-CO_2. In the gas samples of the macro-seep where CO_2 content is small, the δ^{13}C-CO_2 values are close to that of CO_2 at equilibrium with calcite in shales, and do not provide evidence of methane oxidation or OM degradation. On the contrary, the δ^{13}C-CO_2 values obtained by shales degassing (~ −30 to −22 ‰) rather show that the contribution of calcite dissolution to the DIC is significantly lower than the contribution of OM/kerogen/oil degradation and of methane oxidation (Lerouge et al., 2020).

6. Conclusions

The outcropping fractured and slightly weathered "Terres Noires" shales under a thin layer of colluvium (<20 cm) are carbonate-pyrite-bearing claystones rich in organic matter (OM, 4–5 wt%), containing carbonate concretions with oily OM and pyramidal quartz. Weathering is characterized by partial oxidation of pyrite to form gypsum and iron hydroxides. Methane and CO_2 fluxes at the historical macro-seep reach 263 and 1.3 g/m^2/h respectively. A second methane anomaly marked by a higher CH_4 flux of 430 g/m^2/h was detected few meters downslope. Methane prevails (>95 %) in these main emissions together with traces of heavier alkanes (C_2 to C_5) and CO_2. δ^{13}C and δD of methane and C_{2+} alkanes point to a thermogenic origin of the gas, while δ^{13}C of CO_2 suggests microbial degradation of organic matter as the major process of CO_2 formation, at some points CH_4 consumption is a dominant process. The Rochasson macro-seep is representative of a combination of factors favouring greenhouse gas emissions from outcropping black shales worldwide:

(1) Initial organic matter content was high,
(2) total sediment thickness probably exceeded 1 km,
(3) burial led to maturation within the gas window,
(4) subsequent alpine tectonics led to the creation of preferential gas and water migration pathways, within the reservoir and from and to the surface,
(5) uplift brought the reservoir in direct contact with the atmosphere and circulating water,
(6) active and highly dynamic weathering occurs due to the high erosion rates in a young tectonically active mountain range.

Whereas shales cover about 25 % of the land surface (Jin et al., 2014), most recent studies on gas release from black shales have focused on anthropogenic gas emissions (shale gas exploitation). Yet we suspect that, on the global scale, erosion and weathering of organic-rich shales that have undergone relatively recent burial, maturation and uplift in dynamic orogenetic belts can contribute significantly to the greenhouse gas budget. The frequency of methane seeps in the alpine "Terres

Noires" (Gal et al., 2019) seems to support this assumption. For methane, a global estimation of such inputs is lacking. For CO_2, weathering of carbonaceous shales has been estimated to contribute to ~12 % of the estimated annual worldwide flux (Jaffe et al., 2002) but shales can also act as CO_2-sink (Jin et al., 2014). The complex interaction of physical, geochemical, microbial and hydrological boundary conditions in a surface-near shale compartment, as evidenced by our study, needs to be considered when trying to establish realistic gas flux balances, notably based on geochemical or isotopic gas data. The CH_4 flux measured at the Rochasson macro-seep site since 2015 varied with time, by a factor of almost ten, with a maximum in 2019. This illustrates on the one hand the rapidly changing boundary conditions in a young mountainous landscape with highly dynamic erosion (landslides) and hydrology and on the other hand the need of long-term monitoring of similar study sites, to get access to realistic emission rates and also to the endpoints when such emission rates will drop to zero. In this respect, the thermogenic and biogenic components identified in our study need to be considered independently. Whereas the overall quantity of thermogenic gas in the shale reservoir after its burial and uplift is limited, biogenic gas will be continuously produced from the stock of OM in the black shales. The thermogenic gas release will depend on the accessibility of multi-modal nanopores (Ross and Bustin, 2009) by a fractal network of fractures (Vega and Kovscek, 2022) inherited from alpine tectonics. Whereas in the unsaturated nano-pore volume adsorbed gas prevails, gases exist in free or water- or kerogen-dissolved form in open pores and in the fracture network (Xing et al., 2023) so that the dynamics of gas release will depend both on diffusive flow from the pores and on diffusive-advective flow within the fractures. Exhaustion of the considerable thermogenic stock in the Terres Noires formations which may attain several km of thickness (Artru, 1972) has not occurred since their uplift and exposure implying that the gas release proceeded over millions or tens of millions years. Over historical time scales, we have evidence of continuous gas emanation over at least two millenaries for another "eternal flame" the above-mentioned Fontaine Ardente 30 km south of Grenoble in the same Callovo-Oxfordian Terres Noires as the Rochasson seep (Gal et al., 2017). Biogenic gas production is related to more or less superficial shale weathering and will be driven by the dynamics of the erosional front and as such by hydroclimatic conditions, including glaciation-deglaciation cycles, and these processes can be expected to reach their endpoint only at exhaustion of the OM stock or after complete erosion of the formations.

The comprehensive study of all phases, gas, liquid and mineral, present in the Rochasson "Terres Noires" shales, is an opportunity to compare data from direct emissions in the field and those obtained by sample degassing. Gases extracted by rock degassing are less abundant than the gas emitted at the macro-seep. They represent the remnant gas dissolved in pore waters from soils and rocks near the interface with atmosphere. They consist of a major CO_2 component mixed with variable amounts of alkanes and exhibit a wide range of compositions and large isotopic variations of CO_2 and CH_4. These contrasts give evidence of the complex processes that control diffuse gas emissions from weathering shales. Monitoring of all the gas species during the rock degassing provides additional information on gas production and diffusion in the different compartments of soil and shales near the surface (soil, colluvium, outcropping weathered shales and shales at 20–40 cm). The consistency between $\delta^{13}C$-C_{2+} of direct gas emissions from the macro-seep and gases obtained during rock degassing is interesting in two respects. Firstly, from a methodological point of view, the conditions of rock degassing (ambient temperature, long duration until reaching a steady state of gas pressure) allow extracting hydrocarbons without significant isotopic fractionation. Secondly, the C_{2+} data provide evidence of a common source of dissolved and sorbed alkanes of thermogenic origin with RSCM-derived temperatures of ~150 °C, in the colluvium, in surface-near shales and at greater depth, represented by the macro-seep. This implies that the macro-seep is directly fed by the outcropping shale formation. Furthermore, rock degassing and the $\delta^{13}C$ of methane and C_{2+} alkanes in shales provide evidence of the mixing of this thermogenic alkanes with microbial methane (methanogenesis), as well as of methanotrophic microbial activity.

Methanotrophic bacterial activity near the main gas seep can significantly contribute to reducing CH_4 emissions to the atmosphere but adds to CO_2 flux. Shale weathering processes with oxidation of OM need to be considered when investigating the emissions of outcropping, notably for flux estimations. Changes in the isotopic ratios of natural emissions give strong indications on the mechanisms of secondary gas alterations. However, at this point, we can only speculate on the specific microbial pathways involved in methanogenesis and methanotrophic activities ongoing within these shales. Microbial metagenomic approaches in soil/shale samples should further elucidate the strains of microorganisms involved and their active metabolic pathways. Phylogenetic marker genes such as pmoA or mcrA could identify the presence of aerobic or anaerobic methanotrophs, respectively. Clumped isotopic compositions of methane (CH_4 isotopologues) could also give more information on the specific methanogenic pathways ongoing at the site.

CRediT authorship contribution statement

M. Blessing: Writing – review & editing, Writing – original draft, Visualization, Investigation, Conceptualization. **C. Lerouge:** Writing – review & editing, Writing – original draft, Visualization, Supervision, Investigation, Conceptualization. **F. Gal:** Writing – original draft, Visualization, Investigation, Data curation. **A. Lahfid:** Investigation. **C. Fléhoc:** Investigation. **W. Kloppmann:** Writing – review & editing, Project administration, Funding acquisition, Conceptualization.

Declaration of competing interest

The authors declare that they have no known competing financial interests or personal relationships that could have appeared to influence the work reported in this paper.

Acknowledgements

We are grateful to Eric Proust for his help with gas flux measurements and gas sampling during the field campaign and to Benoit Henry for gas concentration analyses. This study was made possible by the financial support from the EU H2020 Programme (grant 764531-SECURe).

Appendix A. Supplementary data

The Supplementary data contains a plan indicating all sampling points and results for gas flux measurements (Figs. S-1, S-2), additional information and details (Fig. S-3) on the applied RSCM method, and a compilation of concentrations of all gaseous species obtained during rock degassing experiments (Tables S1–S3). Supplementary data to this article can be found online at https://doi.org/10.1016/j.scitotenv.2025.179799.

Data availability

Data will be made available on request.

References

Amiel, N., Shaar, R., Sivan, O., 2020. The effect of early diagenesis in methanic sediments on sedimentary magnetic properties: case study from the SE Mediterranean continental shelf. Front. Earth Sci. 8, 283.

Anderson, L.A., 1995. On the hydrogen and oxygen content of marine phytoplankton. Deep-Sea Res. I Oceanogr. Res. Pap. 42 (9), 1675–1680.

Antoine, P., Giraud, A., Meunier, M., Van Asch, T., 1995. Geological and geotechnical properties of the "Terres Noires" in southeastern France: weathering, erosion, solid transport and instability. Eng. Geol. 40 (3–4), 223–234.

Arndt, S., Hetzel, A., Brumsack, H.-J., 2009. Evolution of organic matter degradation in Cretaceous black shales inferred from authigenic barite: a reaction-transport model. Geochim. Cosmochim. Acta 73 (7), 2000–2022.
Artru, P., 1972. Les terres noires du bassin rhodanien (Bajocien supérieur à Oxfordien moyen): stratigraphie, sédimentologie, géochimie, Université Claude Bernard - Lyon I.
Barféty, J.-C., Énay, R., Gidon, M., 1995. L'âge des Terres Noires et des formations associées dans les environs de Grenoble. Géologie alpine 71, 165–168.
Bernard, B., Brooks, J.M., Sackett, W.M., 1977. A geochemical model for characterization of hydrocarbon gas sources in marine sediments, Offshore Technology Conference. OTC, pp. OTC–2934–MS.
Berthier, M., Honegger, J., Eberentz, P., 1991. Etude et travaux pour le renforcement en gaz de la Fontaine Ardente–Commune du Gua (Isère). BRGM report R33584 RHA S, 4.
Blavoux, B., Dazy, J., 1990. Caractérisation d'une province à CO2 dans le bassin du Sud-Est de la France. Hydrogéologie (Orléans) 4, 241–252.
Blessing, M., Proust, E., Fléhoc, C., 2015. Customized injection techniques for compound-specific isotope analysis of natural gas samples. Procedia Earth and Planetary Science 13, 227–231.
Bolton, E.W., Berner, R.A., Petsch, S.T., 2006. The weathering of sedimentary organic matter as a control on atmospheric O2: II. Theoretical modeling. Am. J. Sci. 306 (8), 575–615.
Borrel, G., Jézéquel, D., Biderre-Petit, C., Morel-Desrosiers, N., Morel, J.-P., Peyret, P., Fonty, G., Lehours, A.-C., 2011. Production and consumption of methane in freshwater lake ecosystems. Res. Microbiol. 162 (9), 832–847.
Bott, T., Gregory, S., Shaw, G., Palumbo-Roe, B., 2020. Soil microbial indicators of alkane flux around a natural gas seep. EGU Gen. Assem. Conf. Abstr. 18572.
Bufalo, M., 1989. L'érosion des terres noires dans la région du Buëch (Hautes-Alpes, France), (Aix-Marseille 3).
Cadieux, S.B., White, J.R., Sauer, P.E., Peng, Y., Goldman, A.E., Pratt, L.M., 2016. Large fractionations of C and H isotopes related to methane oxidation in Arctic lakes. Geochim. Cosmochim. Acta 187, 141–155.
Cai, C., Li, H., Li, K., Wang, D., 2022. Thermochemical sulfate reduction in sedimentary basins and beyond: a review. Chem. Geol. 607, 121018.
Chen, C.T.A., Wang, S.L., 1999. Carbon, alkalinity and nutrient budgets on the East China Sea continental shelf. J. Geophys. Res. Oceans 104 (C9), 20675–20686.
Chodzko, J., Lecompte, M., 1992. Ravinement dans les Baronnies. Suivi expérimental. Trav. Lab. Geogr. Phys. (20), 1–109.
Chung, H., Gormly, J., Squires, R., 1988. Origin of gaseous hydrocarbons in subsurface environments: theoretical considerations of carbon isotope distribution. Chem. Geol. 71 (1–3), 97–104.
Clayton, C., Hay, S., Baylis, S., Dipper, B., 1997. Alteration of natural gas during leakage from a North Sea salt diapir field. Mar. Geol. 137 (1–2), 69–80.
Coleman, D.D., Risatti, J.B., Schoell, M., 1981. Fractionation of carbon and hydrogen isotopes by methane-oxidizing bacteria. Geochim. Cosmochim. Acta 45 (7), 1033–1037.
Conrad, R., 2009. The global methane cycle: recent advances in understanding the microbial processes involved. Environ. Microbiol. Rep. 1 (5), 285–292.
Curtis, J.B., 2002. Fractured shale-gas systems. AAPG Bull. 86 (11), 1921–1938.
Debelmas, J., 1978. Un dégagement de gaz naturel dans l'Oxfordien des environs de Grenoble (ravin du Rochasson, commune de Montbonnot, Isère). Géologie alpine 54, 15.
Ding, W., Li, C., Li, C., Xu, C., Jiu, K., Zeng, W., Wu, L., 2012. Fracture development in shale and its relationship to gas accumulation. Geosci. Front. 3 (1), 97–105.
Dzou, L., Milkov, A.V., 2011. Advanced interpretations of stable isotopic composition of gases in working petroleum systems. Search and Discovery Article 90134.
Etiope, G., 2015. Natural gas seepage. In: The Earth's Hydrocarbon Degassing, 199.
Etiope, G., Klusman, R.W., 2002. Geologic emissions of methane to the atmosphere. Chemosphere 49 (8), 777–789.
Etiope, G., Sherwood Lollar, B., 2013. Abiotic methane on earth. Rev. Geophys. 51 (2), 276–299.
Etiope, G., Martinelli, G., Caracausi, A., Italiano, F., 2007. Methane seeps and mud volcanoes in Italy: gas origin, fractionation and emission to the atmosphere. Geophys. Res. Lett. 34 (14).
Etiope, G., Feyzullayev, A., Baciu, C., 2009a. Terrestrial methane seeps and mud volcanoes: a global perspective of gas origin. Marine and Petroleum Geology 26 (3), 333–344.
Etiope, G., Feyzullayev, A., Milkov, A., Waseda, A., Mizobe, K., Sun, C., 2009b. Evidence of subsurface anaerobic biodegradation of hydrocarbons and potential secondary methanogenesis in terrestrial mud volcanoes. Marine and Petroleum Geology 26 (9), 1692–1703.
Etiope, G., Zwahlen, C., Anselmetti, F., Kipfer, R., Schubert, C., 2010. Origin and flux of a gas seep in the Northern Alps (Giswil, Switzerland). Geofluids 10 (4), 476–485.
Etiope, G., Drobniak, A., Schimmelmann, A., 2013. Natural seepage of shale gas and the origin of "eternal flames" in the Northern Appalachian Basin, USA. Marine and Petroleum Geology 43, 178–186.
Gal, F., Kloppmann, W., Proust, E., Bentivegna, G., Defossez, P., Mayer, B., Gaucher, E.C., 2017. Natural CH4 gas seeps in the French Alps: characteristics, typology and contribution to CH4 natural emissions to the atmosphere. Energy Procedia 114 (Supplement C), 3020–3032.
Gal, F., Kloppmann, W., Proust, E., Humez, P., 2018. Gas concentration and flow rate measurements as part of methane baseline assessment: case of the Fontaine Ardente gas seep, Isère, France. Appl. Geochem. 95, 158–171.
Gal, F., Proust, E., Kloppmann, W., 2019. Towards a better knowledge of natural methane releases in the French Alps: a field approach. Geofluids 2019, 1–16.
Giffaut, E., Grivé, M., Blanc, P., Vieillard, P., Colàs, E., Gailhanou, H., Gaboreau, S., Marty, N., Made, B., Duro, L., 2014. Andra thermodynamic database for performance assessment: ThermoChimie. Appl. Geochem. 49, 225–236.
Gong, D., Ma, R., Chen, G., Ma, W., Liao, F., Fang, C., Jiao, L., 2017. Geochemical characteristics of biodegraded natural gas and its associated low molecular weight hydrocarbons. J. Nat. Gas Sci. Eng. 46, 338–349.
Guilhaumou, N., Jouaffre, D., Velde, B.D., Bény, C., 1988. Raman microprobe analysis on gaseous inclusions from the diagenetically altered Terres Noires (SE, France). Bulletin de minéralogie 111 (6), 577–585.
Guilhaumou, N., Touray, J., Perthuisot, V., Roure, F., 1996. Palaeocirculation in the basin of southeastern France sub-alpine range: a synthesis from fluid inclusions studies. Mar. Pet. Geol. 13 (6), 695–706.
Gustafsson, E., Hagens, M., Sun, X., Reed, D.C., Humborg, C., Slomp, C.P., Gustafsson, B. G., 2019. Sedimentary alkalinity generation and long-term alkalinity development in the Baltic Sea. Biogeosciences 16 (2), 437–456.
Hill, D.G., Nelson, C., 2000. Gas productive fractured shales: an overview and update. Gas Tips 6 (3), 4–13.
Hmiel, B., Petrenko, V.V., Dyonisius, M.N., Buizert, C., Smith, A.M., Place, P.F., Harth, C., Beaudette, R., Hua, Q., Yang, B., et al., 2020. Preindustrial 14CH4 indicates greater anthropogenic fossil CH4 emissions. Nature 578 (7795), 409–412.
Hong, W.-L., Etiope, G., Yang, T.F., Chang, P.-Y., 2013. Methane flux from miniseepage in mud volcanoes of SW Taiwan: comparison with the data from Italy, Romania, and Azerbaijan. J. Asian Earth Sci. 65, 3–12.
IAE, 2023. Global Methane Tracker 2023, Paris, pp. IEA (2023), Global Methane Tracker 2023, IEA, Paris. https://www.iea.org/reports/global–methane–tracker–2023 (Licence: CC BY 4.0).
Jaffe, L.A., Peucker-Ehrenbrink, B., Petsch, S.T., 2002. Mobility of rhenium, platinum group elements and organic carbon during black shale weathering. Earth Planet. Sci. Lett. 198 (3–4), 339–353.
James, A., Burns, B., 1984. Microbial alteration of subsurface natural gas accumulations. AAPG Bull. 68 (8), 957–960.
James, R.H., Bousquet, P., Bussmann, I., Haeckel, M., Kipfer, R., Leifer, I., Niemann, H., Ostrovsky, I., Piskozub, J., Rehder, G., 2016. Effects of climate change on methane emissions from seafloor sediments in the Arctic Ocean: a review. Limnol. Oceanogr. 61 (S1), S283–S299.
Jenkyns, H.C., Jones, C.E., GrÖcke, D.R., Hesselbo, S.P., Parkinson, D.N., 2002. Chemostratigraphy of the Jurassic System: applications, limitations and implications for palaeoceanography. J. Geol. Soc. London 159 (4), 351–378.
Jin, L., Ogrinc, N., Yesavage, T., Hasenmueller, E.A., Ma, L., Sullivan, P.L., Kaye, J., Duffy, C., Brantley, S.L., 2014. The CO2 consumption potential during gray shale weathering: insights from the evolution of carbon isotopes in the Susquehanna Shale Hills critical zone observatory. Geochim. Cosmochim. Acta 142, 260–280.
Kietäväinen, R., Purkamo, L., 2015. The origin, source, and cycling of methane in deep crystalline rock biosphere. Front. Microbiol. 6, 725.
Kim, S.-T., O'Neil, J.R., 1997. Equilibrium and nonequilibrium oxygen isotope effects in synthetic carbonates. Geochim. Cosmochim. Acta 61 (16), 3461–3475.
Klusman, R.W., 2018. Faults as windows to monitor gas seepage: application to CO2 sequestration and CO2-EOR. Geosciences 8 (3), 92.
Koch, O., Tscherko, D., Kandeler, E., 2007. Seasonal and diurnal net methane emissions from organic soils of the Eastern Alps, Austria: effects of soil temperature, water balance, and plant biomass. Arct. Antarct. Alp. Res. 39 (3), 438–448.
Krüger, M., van Berk, W., Arning, E.T., Jiménez, N., Schovsbo, N.H., Straaten, N., Schulz, H.-M., 2014. The biogenic methane potential of European gas shale analogues: results from incubation experiments and thermodynamic modelling. Int. J. Coal Geol. 136, 59–74.
Lachassagne, P., Wyns, R., Dewandel, B., 2011. The fracture permeability of hard rock aquifers is due neither to tectonics, nor to unloading, but to weathering processes. Terra Nova 23 (3), 145–161.
Lahfid, A., Beyssac, O., Deville, E., Negro, F., Chopin, C., Goffé, B., 2010. Evolution of the Raman spectrum of carbonaceous material in low-grade metasediments of the Glarus Alps (Switzerland). Terra Nova 22 (5), 354–360.
LaRowe, D.E., Van Cappellen, P., 2011. Degradation of natural organic matter: a thermodynamic analysis. Geochim. Cosmochim. Acta 75 (8), 2030–2042.
Lerouge, C., Grangeon, S., Gaucher, E.C., Tournassat, C., Agrinier, P., Guerrot, C., Widory, D., Fléhoc, C., Wille, G., Ramboz, C., 2011. Mineralogical and isotopic record of biotic and abiotic diagenesis of the Callovian–Oxfordian clayey formation of Bure (France). Geochim. Cosmochim. Acta 75 (10), 2633–2663.
Lerouge, C., Blessing, M., Flehoc, C., Gaucher, E.C., Henry, B., Lassin, A., Marty, N., Matray, J.M., Proust, E., Rufer, D., Tremosa, J., Vinsot, A., 2015. Dissolved CO2 and alkane gas in clay formations. Procedia Earth and Planetary Science 13, 88–91.
Lerouge, C., Robinet, J.-C., Debure, M., Tournassat, C., Bouchet, A., Fernández, A.M., Flehoc, C., Guerrot, C., Kars, M., Lagroix, F., 2018. A deep alteration and oxidation profile in a shallow clay aquitard: example of the Tégulines clay, East Paris Basin, France. Geofluids 2018, 1–20.
Lerouge, C., Debure, M., Henry, B., Fernandez, A., Blessing, M., Proust, E., Made, B., Robinet, J., 2020. Origin of dissolved gas (CO2, O-2, N-2, alkanes) in pore waters of a clay formation in the critical zone (Tegulines Clay, France). Appl. Geochem. 116, 104573.
Lerouge, C., Debure, M., Fernandez, A., Negrel, P., Made, B., Maubec, N., Flehoc, C., Guerrot, C., Blessing, M., Henry, B., Robinet, J., 2023. Hydrogeochemical processes of critical zone developed in Tégulines clay, Paris Basin: Hydrogeochemical and multi-isotopic approach (δ13C, δD, δ18O, 87Sr/86Sr and 14C). J. Hydrol. 617, 129077.
Liu, Y., Zhang, J., Tang, X., 2016. Predicting the proportion of free and adsorbed gas by isotopic geochemical data: a case study from lower Permian shale in the southern North China basin (SNCB). Int. J. Coal Geol. 156, 25–35.

Loyd, S.J., Smirnoff, M.N., 2022. Progressive formation of authigenic carbonate with depth in siliciclastic marine sediments including substantial formation in sediments experiencing methanogenesis. Chem. Geol. 594, 120775.
Ma, Y., Zhong, N., Yao, L., Huang, H., Larter, S., Jiao, W., 2020. Shale gas desorption behavior and carbon isotopic variations of gases from canister desorption of two sets of gas shales in south China. Marine and Petroleum Geology 113, 104127.
Machel, H.G., 2001. Bacterial and thermochemical sulfate reduction in diagenetic settings—old and new insights. Sediment. Geol. 140 (1–2), 143–175.
Maquaire, O., Ritzenthaler, A., Fabre, D., Ambroise, B., Thiery, Y., Truchet, E., Malet, J.-P., Monnet, J., 2002. Caractérisation des profils de formations superficielles par pénétrométrie dynamique à énergie variable: application aux marnes noires de Draix (Alpes-de-Haute-Provence, France). C. R. Geosci. 334 (11), 835–841.
Maquaire, O., Malet, J.-P., Remaıtre, A., Locat, J., Klotz, S., Guillon, J., 2003. Instability conditions of marly hillslopes: towards landsliding or gullying? The case of the Barcelonnette Basin. South East France. Engineering geology 70 (1–2), 109–130.
Mazzini, A., Sciarra, A., Etiope, G., Sadavarte, P., Houweling, S., Pandey, S., Husein, A., 2021. Relevant methane emission to the atmosphere from a geological gas manifestation. Sci. Rep. 11 (1), 4138.
Middelburg, J.J., Soetaert, K., Hagens, M., 2020. Ocean alkalinity, buffering and biogeochemical processes. Rev. Geophys. 58 (3), e2019RG000681.
Milkov, A., Etiope, G., 2018. Revised genetic diagrams for natural gases based on a global dataset of >20,000 samples. Org. Geochem. 125, 109–120.
Milkov, A., Faiz, M., Etiope, G., 2020. Geochemistry of shale gases from around the world: composition, origins, isotope reversals and rollovers, and implications for the exploration of shale plays. Org. Geochem. 143, 103997.
Moss, S., 1992. Organic maturation in the French subalpine chains: regional differences in burial history and the size of tectonic loads. J. Geol. Soc. London 149 (4), 503–515.
Naumenko-Dèzes, M., Kloppmann, W., Blessing, M., Bondu, R., Gaucher, E., Mayer, B., 2022. Natural gas of radiolytic origin: an overlooked component of shale gas. Proc. Natl. Acad. Sci. 119 (15), e2114720119.
Niemann, M., Whiticar, M.J., 2017. Stable isotope systematics of coalbed gas during desorption and production. Geosciences 7 (2), 43.
Olivero, D., Mattioli, E., 2008. The aalenian-Bajocian (Middle Jurassic) of the Digne area. In: Guidebook for the Post-Congress fieldtrip in the Vocontian Basin, SE France (September, 11–13, 2008) 12th Meeting of the International Nannoplankton Association (Lyon, September 7–10, 2008).
Pallasser, R., 2000. Recognising biodegradation in gas/oil accumulations through the δ13C compositions of gas components. Org. Geochem. 31 (12), 1363–1373.
Petsch, S., Berner, R., Eglinton, T., 2000. A field study of the chemical weathering of ancient sedimentary organic matter. Org. Geochem. 31 (5), 475–487.
Prinzhofer, A., Girard, J.P., Buschaert, S., Huiban, Y., Noirez, S., 2009. Chemical and isotopic characterization of hydrocarbon gas traces in porewater of very low permeability rocks: the example of the Callovo-Oxfordian argillites of the eastern part of the Paris Basin. Chem. Geol. 260 (3–4), 269–277.
Rasigraf, O., Vogt, C., Richnow, H., Jetten, M., Ettwig, K., 2012. Carbon and hydrogen isotope fractionation during nitrite-dependent anaerobic methane oxidation by Methylomirabilis oxyfera. Geochim. Cosmochim. Acta 89, 256–264.
Redfield, A.C., Ketchum, B.H., Richards, F.A., 1963. The influence of organisms on the composition of seawater. The sea 2 (2), 26–77.
Rimstidt, J.D., Chermak, J.A., Schreiber, M.E., 2017. Processes that control mineral and element abundances in shales. Earth Sci. Rev. 171, 383–399.
Ross, D.J., Bustin, R.M., 2009. The importance of shale composition and pore structure upon gas storage potential of shale gas reservoirs. Mar. Pet. Geol. 26 (6), 916–927.
Ruppel, C.D., Kessler, J.D., 2017. The interaction of climate change and methane hydrates. Rev. Geophys. 55 (1), 126–168.
Sadezky, A., Muckenhuber, H., Grothe, H., Niessner, R., Pöschl, U., 2005. Raman microspectroscopy of soot and related carbonaceous materials: spectral analysis and structural information. Carbon 43 (8), 1731–1742.
Saspiturry, N., Lahfid, A., Baudin, T., Guillou-Frottier, L., Razin, P., Issautier, B., Le Bayon, B., Serrano, O., Lagabrielle, Y., Corre, B., 2020. Paleogeothermal gradients across an inverted hyperextended rift system: example of the Mauléon fossil rift (Western Pyrenees). Tectonics 39 (10), e2020TC006206.
Saunois, M., Bousquet, P., Poulter, B., Peregon, A., Ciais, P., Canadell, J.G., Dlugokencky, E.J., Etiope, G., Bastviken, D., Houweling, S., et al., 2017. Variability and quasi-decadal changes in the methane budget over the period 2000–2012. Atmos. Chem. Phys. 17 (18), 11135–11161.
Schoell, M., 1980. The hydrogen and carbon isotopic composition of methane from natural gases of various origins. Geochim. Cosmochim. Acta 44 (5), 649–661.
Schovsbo, N.H., Nielsen, A.T., 2017. Generation and origin of natural gas in lower Palaeozoic shales from southern Sweden. GEUS Bull. 38, 37–40.
Seewald, J.S., 2003. Organic–inorganic interactions in petroleum-producing sedimentary basins. Nature 426 (6964), 327–333.
Stolper, D., Lawson, M., Davis, C., Ferreira, A., Neto, E.S., Ellis, G., Lewan, M., Martini, A. M., Tang, Y., Schoell, M., 2014. Formation temperatures of thermogenic and biogenic methane. Science 344 (6191), 1500–1503.
Sugisaki, R., Anno, H., Adachi, M., Ui, H., 1980. Geochemical features of gases and rocks along active faults. Geochem. J. 14 (3), 101–112.
Topp, E., Pattey, E., 1997. Soils as sources and sinks for atmospheric methane. Can. J. Soil Sci. 77 (2), 167–177.
Turchyn, A.V., Bradbury, H.J., Walker, K., Sun, X., 2021. Controls on the precipitation of carbonate minerals within marine sediments. Front. Earth Sci. 9, 618311.
Tyson, R., 1987. The genesis and palynofacies characteristics of marine petroleum source rocks. Geol. Soc., London, Spec. Publ. 26 (1), 47–67.
Vega, B., Kovscek, A.R., 2022. Fractal characterization of multimodal, multiscale images of shale rock fracture networks. Energies 15 (3), 1012.
Venturi, S., Tassi, F., Cabassi, J., Randazzo, A., Lazzaroni, M., Capecchiacci, F., Vietina, B., Vaselli, O., 2021. Exploring methane emission drivers in wetlands: the cases of Massaciuccoli and Porta Lakes (Northern Tuscany, Italy). Appl. Sci. 11 (24), 12156.
Vinson, D.S., Blair, N.E., Martini, A.M., Larter, S., Orem, W.H., McIntosh, J.C., 2017. Microbial methane from in situ biodegradation of coal and shale: a review and reevaluation of hydrogen and carbon isotope signatures. Chem. Geol. 453, 128–145.
Wang, X., Li, X., Wang, X., Shi, B., Luo, X., Zhang, L., Lei, Y., Jiang, C., Meng, Q., 2015. Carbon isotopic fractionation by desorption of shale gases. Marine and Petroleum Geology 60, 79–86.
Wang, Z., Zeng, D., Patrick, W.H., 1996. Methane emissions from natural wetlands. Environ. Monit. Assess. 42, 143–161.
Whiticar, M.J., 1999. Carbon and hydrogen isotope systematics of bacterial formation and oxidation of methane. Chem. Geol. 161 (1–3), 291–314.
Whiticar, M.J., Faber, E., Schoell, M., 1986. Biogenic methane formation in marine and freshwater environments: CO2 reduction vs. acetate fermentation—isotope evidence. Geochim. Cosmochim. Acta 50 (5), 693–709.
Wopenka, B., Pasteris, J.D., 1993. Structural characterization of kerogens to granulite-facies graphite: applicability of Raman microprobe spectroscopy. Am. Mineral. 78 (5–6), 533–557.
Xing, Y., Xiao, X., Zhou, Q., Liu, W., Zhao, Y., 2023. Influence of water on the methane adsorption capacity of organic-rich shales and its controlling factors: a review. Energies 16 (8), 3305.